EUMETSAT Satellite Application Facility on
Support to Operational Hydrology and Water Management

Algorithm Theoretical Baseline Document (ATBD) for product H01 new rel. (PR-OBS-1 new rel.)

Precipitation rate at ground by MW conical scanners

Reference Number:	SAF/HSAF/ATBD-01 new rel.
Issue/Revision Index:	2.1
Last Change:	31 May 2013

DOCUMENT CHANGE RECORD

Issue / Revision	Date	Description
1.0	16/05/2011	Baseline version prepared for ORR1 Part 2
1.1	16/05/2011	Updates, acknowledging ORR1 Part 2 review board recommendation
2.0	23/04/2013	Major release including section "PR-OBS-01 Delta Validation (2013)" prepared for ORR 1 Part 3 - Delta
2.1	31/05/2013	Acknowledged updates coming from reviewers' comments of ORR1 Part3-Delta: • Introduction of section 2.4 for explanation of changes introduced with the new product version • Change on title

Index

List of Figures

List of Tables

Acronyms

AMSU	Advanced Microwave Sounding Unit (on NOAA and MetOp)
AMSU-A	Advanced Microwave Sounding Unit - A (on NOAA and MetOp)
AMSU-B	Advanced Microwave Sounding Unit - B (on NOAA up to 17)
ATBD	Algorithms Theoretical Basline Document
AU	Anadolu University (in Turkey)
BfG	Bundesanstalt für Gewässerkunde (in Germany)
CAF	Central Application Facility (of EUMETSAT)
CDOP	Continuous Development-Operations Phase
CESBIO	Centre d'Etudes Spatiales de la BIOsphere (of CNRS, in France)
CM-SAF	SAF on Climate Monitoring
CNMCA	Centro Nazionale di Meteorologia e Climatologia Aeronautica (in Italy)
CNR	Consiglio Nazionale delle Ricerche (of Italy)
CNRS	Centre Nationale de la Recherche Scientifique (of France)
DMSP	Defense Meteorological Satellite Program
DPC	Dipartimento Protezione Civile (of Italy)
EARS	EUMETSAT Advanced Retransmission Service
ECMWF	European Centre for Medium-range Weather Forecasts
EDC	EUMETSAT Data Centre, previously known as U-MARF
EUM	Short for EUMETSAT
EUMETCast	EUMETSAT's Broadcast System for Environmental Data
EUMETSAT	European Organisation for the Exploitation of Meteorological Satellites
FMI	Finnish Meteorological Institute
FTP	File Transfer Protocol
GEO	Geostationary Earth Orbit
GRAS-SAF	SAF on GRAS Meteorology
HDF	Hierarchical Data Format
HRV	High Resolution Visible (one SEVIRI channel)
H-SAF	SAF on Support to Operational Hydrology and Water Management
IDL©	Interactive Data Language
IFOV	Instantaneous Field Of View
IMWM	Institute of Meteorology and Water Management (in Poland)
IPF	Institut für Photogrammetrie und Fernerkundung (of TU-Wien, in Austria)
IPWG	International Precipitation Working Group
IR	Infra Red
IRM	Institut Royal Météorologique (of Belgium) (alternative of RMI)
ISAC	Istituto di Scienze dell'Atmosfera e del Clima (of CNR, Italy)
ITU	İstanbul Technical University (in Turkey)
LATMOS	Laboratoire Atmosphères, Milieux, Observations Spatiales (of CNRS, in France)
LEO	Low Earth Orbit
LSA-SAF	SAF on Land Surface Analysis
Météo France	National Meteorological Service of France
METU	Middle East Technical University (in Turkey)
MHS	Microwave Humidity Sounder (on NOAA 18 and 19, and on MetOp)
MSG	Meteosat Second Generation (Meteosat 8, 9, 10, 11)
MVIRI	Meteosat Visible and Infra Red Imager (on Meteosat up to 7)
MW	Micro Wave
NESDIS	National Environmental Satellite, Data and Information Services
NMA	National Meteorological Administration (of Romania)
NOAA	National Oceanic and Atmospheric Administration (Agency and satellite)
NWC-SAF	SAF in support to Nowcasting & Very Short Range Forecasting
NWP	Numerical Weather Prediction
NWP-SAF	SAF on Numerical Weather Prediction
O3M-SAF	SAF on Ozone and Atmospheric Chemistry Monitoring

OMSZ	Hungarian Meteorological Service
ORR	Operations Readiness Review
OSI-SAF	SAF on Ocean and Sea Ice
PDF	Probability Density Function
PEHRPP	Pilot Evaluation of High Resolution Precipitation Products
Pixel	Picture element
PMW	Passive Micro-Wave
PP	Project Plan
PR	Precipitation Radar (on TRMM)
PUM	Product User Manual
PVR	Product Validation Report
RMI	Royal Meteorological Institute (of Belgium) (alternative of IRM)
RR	Rain Rate
RU	Rapid Update
SAF	Satellite Application Facility
SEVIRI	Spinning Enhanced Visible and Infra-Red Imager (on Meteosat from 8 onwards)
SHMÚ	Slovak Hydro-Meteorological Institute
SSM/I	Special Sensor Microwave / Imager (on DMSP up to F-15)
SSMIS	Special Sensor Microwave Imager/Sounder (on DMSP starting with S-16)
SYKE	Suomen ympäristökeskus (Finnish Environment Institute)
T_{BB}	Equivalent Blackbody Temperature (used for IR)
TKK	Teknillinen korkeakoulu (Helsinki University of Technology)
TMI	TRMM Microwave Imager (on TRMM)
TRMM	Tropical Rainfall Measuring Mission UKMO
TSMS	Turkish State Meteorological Service
TU-Wien	Technische Universität Wien (in Austria)
U-MARF	Unified Meteorological Archive and Retrieval Facility
UniFe	University of Ferrara (in Italy)
URD	User Requirements Document
UTC	Universal Coordinated Time
VIS	Visible
ZAMG	Zentralanstalt für Meteorologie und Geodynamik (of Austria)

1 Introduction to product PR-OBS-1

1.1 Sensing principle

Product PR-OBS-1 is fundamentally based on the instruments SSM/I and SSMIS flown on the DMSP satellites. These conical scanners provide images with constant zenith angle, that implies constant optical path in the atmosphere and homogeneous impact of the polarisation effects (see next figure).

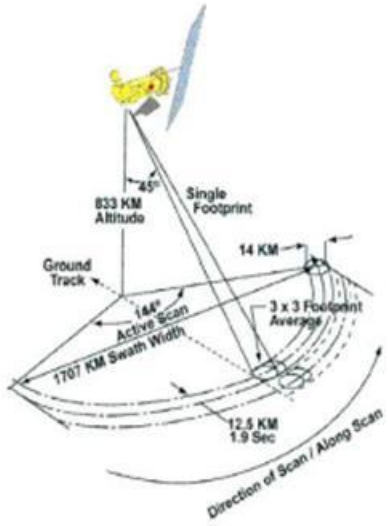

Figure 1 Geometry of conical scanning for SSMIS

Also, conical scanning provides constant resolution across the image, though changing with frequency. It is noted that the IFOV is elliptical, with major axis elongated along the viewing direction and the minor axis along-scan, approximately 3:5 of the major. Its size is dictated by the antenna diameter (actually, the antenna is slightly elliptical, to partially compensate for the panoramic distortion), but also by the portion of antenna effectively illuminated (this enables to obtain the same IFOV for a group of different frequencies, if co-registration is a strong requirement). As for the 'pixel', i.e. the area subtended as a consequence of the bi-dimensional sampling rate, the sampling distance along the satellite motion, i.e. from scan line to scan line, is invariably 12.5 km, dictated by the satellite velocity on the ground and the scan rate. Along scan, the sampling rate is selected differently for different frequencies or set of frequencies, as necessary to fulfil the radiometric accuracy requirement and to minimise aliasing.

For more information, please refer to the Products User Manual (specifically, volume PUM-01).

1.2 Main operational characteristics

The operational characteristics of PR-OBS-1 are discussed in PUM-01. Here are the main highlights.

The horizontal resolution (Δx). The IFOV of SSM/I-SSMIS images changes with frequency from ~ 15 km at 90 GHz to ~ 55 km at 19 GHz). We consider the 90 GHz channel IFOV 13.2 x 15.5 km, as effective for most precipitation types. Sampling is performed at ~ 12.5 km intervals. Thus:

- resolution Δx 13.2 x 15.5 km - sampling distance: 12.5 km.

The *observing cycle (Δt)* depends on the instrument swath and the number of satellites carrying the addressed instrument. For PR-OBS-1 there are 4 DMSP satellites but, because of the limited

instrument swath, they provide a total service equivalent to that one of two satellites, around 7:00 and 18:00 LST. In average the observing cycle over Europe is $\Delta t \sim 6$ h, with actual interval ranging from 2 to 10 hours. Gaps are filled by product PR-OBS-2, that also has observing cycle $\Delta t \sim 6$ h, but LST around 9:30 and 14:00, with actual intervals ranging from 4.5 to 7.5 hours. Conclusion:

- for PR-OBS-1 as stand alone (i.e. from DMSP satellites): cycle $\Delta t = 6$ h, sampling 2÷10 h;
- for the composite PR-OBS-1 + PR-OBS-2 system: cycle $\Delta t = 3$ h, sampling 2÷4.5 h.

The *timeliness (δ)* is defined as the time between observation taking and product available at the user site assuming a defined dissemination mean. The timeliness depends on the satellite transmission facilities, the availability of acquisition stations, the processing time required to generate the product and the reference dissemination means. In the case of PR-OBS-1 it is strongly conditioned by the availability of DMSP data at CNMCA, through NOAA and UKMO. The outcome is

- timeliness $\delta \sim 2.5$ h.

The *accuracy (RMS)* is the convolution of several measurement features (random error, bias, sensitivity, precision, …). To simplify matters, it is generally agreed to quote the root-mean-square difference [observed - reference values]. The accuracy of a satellite-derived product descends from the strength of the physical principle linking the satellite observation to the natural process determining the parameter. It is difficult to be estimated *a-priori*: it is generally evaluated *a-posteriori* by means of the validation activity.

1.3 Architecture of the products generation chain

The architecture of the PR-OBS-1 product generation chain is shown in next Figure:

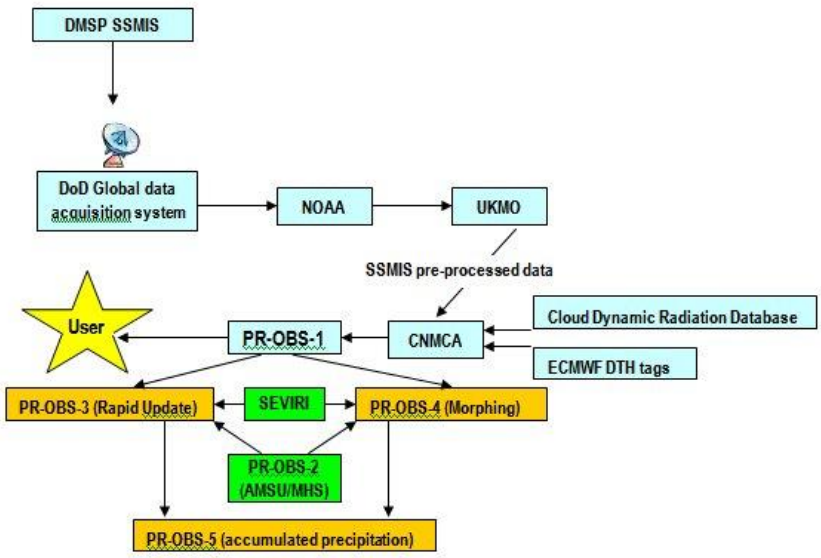

Figure 2 Architecture of the PR-OBS-1 product generation chain

A main feature of the architecture of PR-OBS-1 is the unavailability of DMSP data by direct reception or by EUMETCast. This strongly conditions the timeliness for product delivery. The data are acquired

within the DoD system for global DMSP data, and conveyed to NOAA, that re-transmits them to the UK Meteorological Office (UKMO). CNMCA acquires the data from UKMO already pre-processed.

The figure reminds that the PR-OBS-1 product, in addition to be disseminated to the users, is also used internally to CNMCA to feed the frequent Rapid-Update product (PR-OBS-3) and Morphing product (PR-OBS-4).

In CNMCA, the PR-OBS-1 product is generated on the base of the algorithms and the databases developed and provided by CNR-ISAC.

The product, that includes some online quality control information, is disseminated to the Users by FTP.

1.4 Changes introduced with the new product version

The version 1.7 of PR-OB-1 algorithm is characterized by several new features with respect to its previous versions. They include: the increased horizontal resolution of the surface precipitation rate (which now corresponds to the IFOV of the high frequency channels of SSMIS, i.e., 13.2 km x 15.5 km), the upgrade of the screening procedure of non-precipitating pixels to achieve consistency with PR-OBS-2 (ver. 2.4) (see Section 3.5) and the retrieval of the phase of the precipitation (see Section 3.6). A major improvement of version 1.7 is the upgrade of the dynamical/meteorological component in the database used in the retrieval procedure (see Section 3.4). Four dynamical variable have been considered: Omega (vertical motion) at 700 mb , CAPE, Moisture flux close to the surface, and Freezing level height, and they are extracted from the oprational ECMWF forecast at 3 or 6 hours. Another major improvement, which will have substantial effects in the future on the validation results, is the determination of a pixel based quality flag (or percentage of confidence index) to be associated to the precipitation retrieval (see Section 3.6).

2 Processing concept

2.1 Instrument data structure

Product PR-OBS-1 is fundamentally based on SSM/I and SSMIS. These conical scanners provide images with constant zenith angle, implying constant optical path in the atmosphere and homogeneous impact of the polarisation effects.

Also, conical scanning provides constant resolution across the image, though changing with frequency. It is noted that the IFOV is elliptical, with major axis elongated along the viewing direction and the minor axis along-scan, approximately 2/3 of the major. Its size is dictated by the antenna diameter (actually, the antenna is slightly elliptical, to partially compensate for the panoramic distortion), but also by the portion of antenna effectively illuminated (this enables to obtain the same IFOV for a group of different frequencies, if co-registration is a strong requirement). As for the 'pixel', i.e. the area subtended as a consequence of the bi-dimensional sampling rate, the sampling distance along the satellite motion, i.e. from scan line to scan line, is invariably 12.5 km, dictated by the satellite velocity on the ground and the scan rate. Along scan, the sampling rate is selected differently for different frequencies or set of frequencies, as necessary to fulfil the radiometric accuracy requirement and to minimise aliasing.

To 'rasterise' this complicated sequence of pixels stemming from the conical scanning geometry so that it can be easily accessed from the precipitation processing chain, and to apply all necessary co-registration and calibration operations, also accounting for the actual satellite/instrument attitude and housekeeping, is not an easy task. An 'instrument processor' performs this task, considered as a black-box procured from external sources, thus not be described in this ATBD.

2.2 Introduction to the SSMIS processing chains

In PR-OBS-1 (ver. 1.7) only SSMIS is processed, since data from the last SSM/I (F15) are no longer available (officially in "degraded" status). SSMIS includes all 'window' channels of SSM/I (19, 37 and 90 GHz with two polarisations) and the water-vapour channel (23 GHz) for water vapour correction, with pixel 25 x 12.5 km^2 (19, 23 and 37 GHz) and 12.5 x 12.5 km^2 (90 GHz). SSMIS adds a set of channels with pixel 37.5 x 12.5 km^2, for temperature profile in the troposphere (8 channels between 50.3 and 60.8 GHz) and water vapour profile (4 channels: 150 GHz and 3 channels in the 183 GHz band). Further 5 channels in the interval 60.8 to 63.3 GHz, with pixel 75 x 12.5 km^2, are for stratospheric temperature profile, probably of no interest for precipitation retrieval.

Determining precipitation rate at the ground from SSMIS is an ill-conditioned problem. The precipitation at the ground, that in no way can be directly observed from space, is derived from the knowledge of everything that happens in the vertical column, specifically in terms of hydrometeors. SSMIS includes more information on the vertical atmospheric structure than SSM/I,. Channels in the 54 GHz and 183 GHz bands can provides important clues about factors such as temperature profile, water vapour profile, cloud-top height, since each channel is sensitive to a specific layer of the atmosphere, Consequently, information on cloud microphysics needs to be input from external. There are two approaches for this.

- To assimilate MW brightness temperature (T_B) in a NWP model that provides information on cloud microphysics. This is the approach of ECMWF. The problem is that real-time assimilation currently is only possible with coarse-resolution models ('coarse' in relative terms in respect of the convection scale). These models cannot retrieve microphysical parameters with the

necessary degree of detail, and tend to smooth-out extreme events. This approach is probably suitable for the global scale, at least from the statistical viewpoint.

- Microphysical parameters are conveniently retrieved by Cloud Resolving Models (CRM). The problem here is that it is currently not possible to run these models in-line with the flow of satellite data. It is therefore necessary to do this off-line, for a number of well-documented events (generally, results of re-analysis exercises) and collect the results in a database. This also allows using more complex Radiative Transfer Models (RTM), as it is particularly necessary when ice is involved in the precipitation event. The collection of samples of meteorological events, with added cloud microphysics and dynamical/meteorological information by the CRM, and converted into T_B's at the instrument channel frequencies by the RTM, constitutes the Cloud Dynamics Radiation Database (CDRD).

In the deep future, when it will be possible to run CRM's assimilating the satellite data flow in-line, the first approach could prevail. For the moment, we have adopted the second approach, that is currently considered the most advanced. It was originally developed for SSM/I, then it has been extensively used after the launch of the TRMM satellite to process the data from TMI (a special configuration of SSM/I), and it is presently baselined for processing the data from the GPM mission to come.

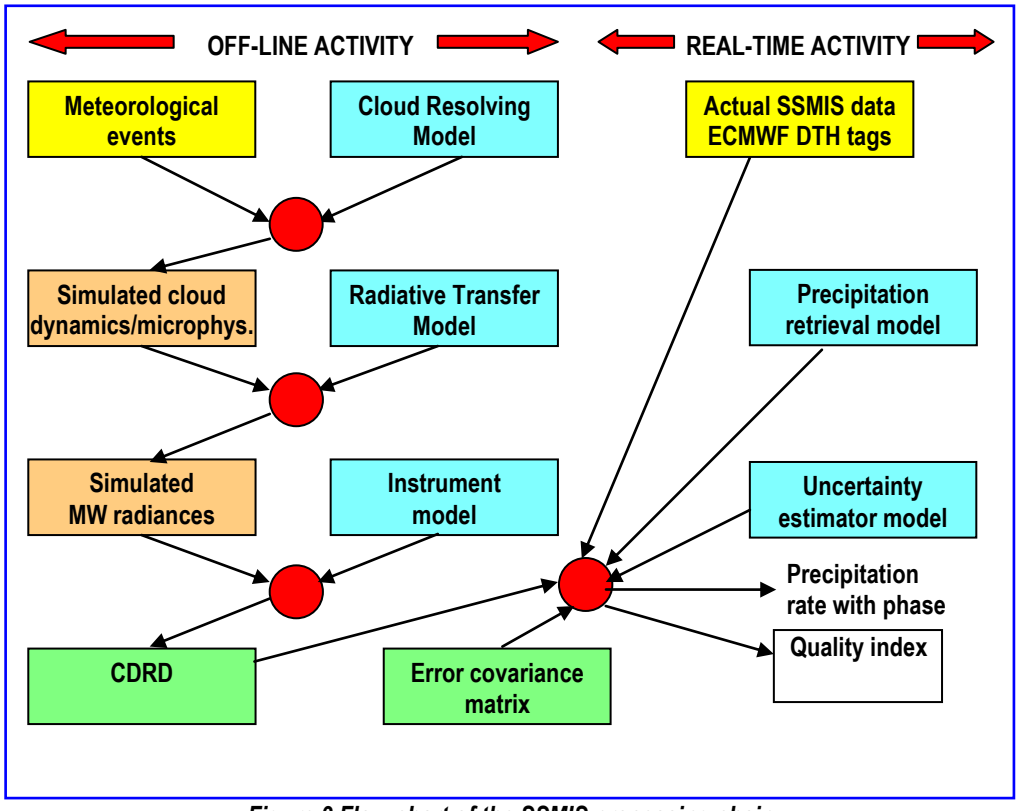

Figure 3 Flow chart of the SSMIS processing chain

Figure above illustrates the flow chart of the SSMIS processing chain, which is maintained for the PR-OBS-1 (ver. 1.7). The off-line part refers to the activities leading to implement the Cloud Dynamics Radiation Database. They consist of:

- collecting well-documented meteorological events (analysis or re-analysis);

- applying a Cloud Resolving Model to simulate the cloud microphysics missing in the analysis and providing the dynamical/meteorological information to be associated to each simulated cloud microphysical structure;
- applying a Radiative Transfer Model to convert the cloud pattern in a pattern of (monochromatic) radiances at all frequencies and polarisations of the SSMIS channels;
- convoluting the monochromatic radiances with the instrument model so to simulate brightness temperatures comparable with those that would be measured from the satellite;
- finally collect the simulated T_B's in the Cloud-Radiation Database.

When the satellite passes, the acquired SSMIS data are pre-processed by the instrument processor. The ECMWF global forecast model output at 0.5 degrees closest in time of the SSMIS overpass at each location, provides the optimal dynamical/thermodynamical/hydrological constraint parameters (DTH tags) to be associated to the SSMIS observations. These data are made available for the precipitation generation chain, that includes:

- an initial preparation of the dataset to be processed (sea-land mask, emissivity, selection of portion of database based on ECMWF DTH tags, …)
- the retrieval algorithm that searches for the maximum-likelihood solution in the hydrometeor profiles available in the selected portion of the CDRD, also using the error structure available in a database;
- the precipitation rate is associated to a quality flag and a phase flag.

3 Algorithms description

The following Sections describe the algorithms used in the various modules of the precipitation products generation chain. The degree of detail is consistent with the requirement of a manageable document.

3.1 The Cloud Resolving Model

A meteorological situation (analysis or re-analysis) is generally described in terms of parameters measured by the ground-based or the space-based observing system. These parameters do not generally include the details of the cloud structure, specifically the cloud microphysical structure that determines precipitation. This will to be reconstructed by applying an atmospheric model. We will make use of the "***University of Wisconsin – Non-hydrostatic Modeling System***" (***UW-NMS***).
The UW-NMS model represents the further development of the regional atmospheric modelling system maintained at Colorado State University (see Tripoli and Cotton 1981, 1982, 1986; Cotton et al. 1982, 1986; Tripoli 1992 a,b) with more recent major improvements concerning the model's dynamical conservation properties and its unique variable step topography (VST) surface coordinate system described by Tripoli and Smith (2012). The NMS is a 3-dimensional, nonhydrostatic, nested, scalable regional-mesoscale, prognostic model. It is able to simulate atmospheric phenomena across all relevant scales from microscale, up through mesoscale and out to the synoptic/regional scales. This model is chosen because of its ability to achieve accuracy in simulating scale-interaction processes through imposition of conservation on mass, energy, momentum, vorticity and enstrophy throughout model integration. The underlying model framework uses quasi-compressible closure formulated on an Arakawa "C" grid cast on multiple-nest rotated spherical grids using multiple two-way nesting. The model employs non-Boussinesq dynamics, two-way grid nesting exchanges, and a unique terrain-following VST vertical coordinate system at its lower boundary. The two-way interactive nesting scheme allows increased resolution in focused areas. VST coordinates are able to capture the dynamical consequences of either steep inclinations or subtly varying terrain features without sacrificing accuracy for any type of terrain-induced slope flows at any scale as shown in Tripoli and Smith (2012). A variable ice-liquid water potential temperature is used as the predictive thermodynamic variable in the model (Tripoli and Cotton 1981). The advantage in using this quantity is its conserved properties for all phase changes. In so doing, potential temperature, water vapor and cloud water are all treated as diagnostic variables.

The UW-NMS microphysical module used for this study is a modified form of the scheme described by Flatau et al. (1989) and Cotton et al. (1986), and more recently improved by Panegrossi (2004). Specifically, in UW-NMS the treatment of ice categories and specifics of the precipitation physics tendencies has been modified from the original published works to enhance their performance. The microphysics is a bulk microphysics parameterization, which includes six hydrometeor categories labelled as: suspended cloud droplets, precipitating rain drops, suspended pristine ice crystals, and precipitating low-density graupel particles (or snow pellets), ice aggregates and high-density graupel particles. Depending on the application, all or some of these categories may be selected. Any combination of frozen and liquid hydrometeors can coexist within the same grid volume at any given time to allow hydrometeor category interaction to take place.

A negative exponential size distribution *N(D)* is assumed for all categories (except cloud droplets and pristine crystals, which are considered monodispersed), and it is given by:

$$N(D) = N_0 e^{-\lambda D}$$

where N_0 is the intercept and λ is the slope of the distribution. The total concentration of hydrometeors in the distribution can be found by an integration of the distribution:

$$N_t = \int_0^\infty N(D)dD = N_0 / \lambda$$

The mean diameter and the liquid water content are quantities frequently used in cloud modelling applications. The mean diameter D_m is the first moment of the distribution, and it is defined as:

$$D_m = \frac{\int_0^\infty DN(D)dD}{\int_0^\infty N(D)dD}$$

For a negative exponential it becomes:

$$D_m = \frac{1}{\lambda}$$

The liquid water content or ice water content is proportional to the third moment of the distribution:

$$l_h = \int_0^\infty m(D)N(D)dD$$

where *m(D)* is the mass of particles of diameter D. For spherical particles of density ρ_h with negative-exponential size distribution, it becomes:

$$l_h = \pi N_t D^3 m \rho_h$$

An alternative to the liquid water content to describe the mass content of hydrometeors within the cloud is the mixing ratio defined as:

$$r_h = \frac{l_h}{\rho_0}$$

where ρ_0 is the dry air density. It is always predicted in UW-NMS, and it is related to the size distribution parameters by:

$$\lambda = \left[\frac{\pi \rho_h N_t}{\rho_0 r_h} \right]^{\frac{1}{3}}$$

One can see that the distribution can be completely described by assigning a value of either the slope, or the intercept, or the concentration. The model always predicts the total mixing ratio of all condensate (liquid and ice), water vapor mixing ratio, and the mixing ratio of each hydrometeor category, except for cloud droplets whose mixing ratio is diagnosed.

For each hydrometeor category, the UW-NMS model offers the possibility to specify the value either for the slope, or for the intercept, or for the total number concentration. A different method for parameterising each hydrometeor category can be selected where the total concentration (number of particles per unit mass) can be predicted. This option allows the parameters of the size distribution λ and N_0 to be diagnosed from the mixing ratio and the total concentration, obtaining different values of

the slope and the intercept at each grid volume. Mixed-phase particles (i.e. melting graupel) are not included but any combination of liquid and frozen particles is allowed to occur at a given grid point.

For the aim of this project it is very important to describe the parameterization of each hydrometeor category, explaining the major assumptions in the conversion process between one category and the other, and to describe the parameterization of their microphysical properties. Particular emphasis will be given below to the size distribution and density (for the frozen hydrometeors) parameterization, because these are the parameters that directly determine the optical properties.

A - Cloud droplets - The cloud water drops are assumed to be of constant size except with respect to the formulations for autoconversion and ice splintering where they are cast in the form of a modified Gamma distribution (Tripoli and Cotton 1981). Their mixing ratio is diagnosed, while their concentration is specified *a priori* since cloud water nucleation is not explicitly considered in the model. The typical characteristic diameter (D_C) of cloud droplets is 0.02 mm with the density of pure water (ρ_w), *i.e.*, 1 g cm^{-2}. Besides the implicit diffusional growth and decay of cloud water due to production of supersaturation built into a diagnostic system, cloud water may be converted to any of the other hydrometeor categories through collection, phoretic contact freezing, or autoconversion directly to rain. Stochastic broadening is parameterized to be dependent on the average cloud-droplet size.

B - Rain drops – For this study, the rain water category is assumed to be distributed in a Marshall-Palmer distribution of specified constant intercept of 0.08 cm^{-4}. Rain droplets arise primarily through the collision-coalescence process (warm rain) and the melting of precipitating ice particles (cold rain). In warm-based clouds, like those typical of summertime Alabama or tropical cyclone, both processes are important. Rain droplets are lost to the system primarily through conversion to ice categories (droplet freezing and riming) or evaporation and through loss due to precipitation.

C - Pristine ice crystals - The original pristine ice category of the Flatau parameterization (Flatau et al. 1989) is divided into a snow and pristine category. The original version grouped both nucleated and new crystals together. Since a constant size distribution had been assumed, massive nucleation at cold temperatures would drastically alter the average crystal size and would remove all memory of the growth that some of the larger crystals had been through. Here, riming growth processes are assumed to convert pristine crystals at their predicted mass to a snow category which represents rimed crystals. Hence, new and mature populations of crystals continue to exist as pristine crystals where massive nucleation occurres, whereas crystals that have substantially increased in mass through riming are separated out in can evolve independently. This was specially important for the simulations of cirrus anvils where influxes of pristine crystals would dominate the old inclusive pristine category sometimes preventing the precipitation of the rimed particles . Both their concentration and mixing ratio are predicted, therefore their mass and size change at each grid point, with a typical D_C of ~0.24 mm. The density (ρ_p) is derived according to Flatau et al. (1989) starting with a mass - diameter (m - D) relationship:

$$D = \beta \left(\frac{m}{K} \right)^{\alpha}$$

where α is a non-dimensional exponential factor, β is a size scale factor (in cm) and K is a mass normalization factor (in g). For an equivalent volume sphere, the density becomes:

$$\rho_p = \frac{6}{\pi} K \beta^{\alpha} D^{1/\alpha - 3}$$

The three parameters, α *(=0.5)*, β (=19.2 cm) and K *(=1g)* depend on the crystal mass in such a manner that as the mass (or size) increases, the density decreases (see Casella et al., 2013 and Smith et al., 2013 for further details). The only source of new crystals are primary and secondary nucleation

including sorption and deposition, contact nucleation and splintering. Pristine crystals can be lost through conversion to hard graupel resulting from collection directly onto the graupel surface or through contact freezing of rain droplets, by conversion to soft graupel through the riming of cloud droplets or the conversion to aggregates through the aggregation process. Because pristine ice crystals tend to remain quite small in mass, they can be assumed to melt instantaneously when the temperature of the air exceeds freezing.

D - Ice aggregates / Snowflakes - The aggregate category consists of aggregated crystals formed by collisions among pristine crystals, or pristine crystals other aggregates. Aggregates are assumed to be in a Marshall-Palmer distribution of constant assumed slope, with mean radius of 1650 μm. The implicit assumption is that break-up balances formation. Additional growth is possible from riming and deposition, although strong riming will result in conversion to graupel at a specified rate. Aggregates represent the major source of graupel embryos. Aggregates are lost to melting, evaporation, precipitation fallout processes and conversion to snow pellets through riming processes. For aggregates the size dependent density $\rho_{s/a}$ is given the above equations, where α = 0.419 and β = 8.89 cm. The resultant expression is is $\rho_a (D_C)$ = 0.015 / [$D_C^{0.6}$] g cm^{-3} (Panegrossi et al., 1998)

E - Soft graupel / Snow pellets - The snow pellets (or soft graupel) category is assumed to follow a Marshall-Palmer distribution with constant intercept of 0.014 cm^{-4}. The snow pellets are assumed to grow from their initiation size through vapour-deposition processes and riming of both rain and cloud droplets. There is an assumed conversion formula to convert the soft graupel to the hard graupel category, which is dependent on the riming rate by rain droplets compared to growth rates by other processes and the relative size of collected rain droplets compared to the snow particle size.

Snow represents soft, low-density ice forming when pristine crystals or aggregates become heavily rimed, with their density (ρ_s) formulated according to Macklin (1962):

$$\rho_s = \left(-\frac{\hat{r}\hat{U}_{imp}}{T_s} \right)^b$$

in which T_S is the surface temperature of the ice substrates (in ℃), $\hat{r}$ is a weighted averaged radius (in μm) and $\hat{U}_{imp}$ is the weighted average impact velocity of cloud droplets and rain drops (in $m\ s^{-1}$). The values for the *a* and *b* coefficients are 0.23 g cm^{-3} and 0.44, respectively, as reported by Prodi *et al.* (1991). The $\hat{r}$ is calculated by averaging the radii of the cloud droplet and rain drop diameters, weighted by their respective mixing ratios. The $\hat{U}_{imp}$ is calculated by averaging the impact velocity between rain drops and snow (*i.e.*, the difference between the terminal velocities of rain drops and snow) with the impact velocity between cloud droplets and snow (*i.e.*, approximately the terminal velocity of snow alone), again weighted by the mixing ratios of cloud droplets and rain drops. The resultant snow density typically covers a range of values from 0.05 - 0.9 g cm^{-3}.

F - Hard graupel / Hailstones - The hard graupel category is also assumed to be in a constant intercept (0.071 cm^{-4}) Marshall-Palmer distribution and constant density ρ = 0.9 g/cm^3. Hard graupel grows or decays from vapour deposition, riming, and melting and conversion from rain, pristine crystals, aggregates and soft graupel categories. Wet growth or dry growth are both modeled and depend on the diagnosed equilibrium temperature of the graupel surface. This temperature depends of the energy balance at the surface of the droplet resulting from conduction with the air versus latent heating or cooling due to evaporation or sublimation onto the particle, and freezing of collected liquid water. At sub freezing, air temperatures, the energy balance determines the proportion of any collected liquid water that can be frozen, given the rate that the particle can conduct heat away to the air. Any excess water that cannot freeze is assumed to be shed as rain. Hence wet or dry growth or melting is modeled at below or above freezing temperatures dependent on the diagnosed

energy balance. The results of this balance can be made available for radiative transfer calculations since the existence of a liquid coating dramatically alters radiative properties of the graupel particle.

3.2 The Radiative Transfer Model

An accurate and efficient radiative transfer equation (RTE) model is essential to transform the CRM-generated meteorological and microphysical information into upwelling passive microwave TBs that are to be included into the simulation database. The multiple scattering solution we use within the RMS to develop the CDRD database is a one-dimensional plane-parallel Eddington approximation to the inelastic, steady-state RTE (see Liou, 2002]). Further refinements for applications with the RTE model take into account cloud microphysical specifications used with respect to the CRM, refinements which are discussed below.

The plane-parallel Eddington approximation is well known and widely used especially because of its computational efficiency. It is important to recognize that for the most part, the mean PMW TB differences between a one-dimensional RTE model and fully three-dimensional RTE model (either through use of an analytical approximation scheme or a generalized Monte Carlo method) are within a few degrees in magnitude (see Roberti et al., 1994, Smith et al, 2002) even considering the use of the higher SSMIS frequencies (see Bauer et al., 2006). Although these differences may become significant locally in case of strong horizontal gradients within the cloud microphysical properties such as near cloud edges (*e.g.*, Liu et al., 1996), we have found in our own calculations that the treatment of the optical properties of the ambient hydrometeors and their concomitant treatment in a single scatter framework is far more important in reconciling RTE model calculations with satellite observations, than the particular choice of the core RTE model solution. The last argument is in accordance with the recent study of Kulie et al. (2010) based on several ice scattering models compared within the framework of both passive and active microwave models.

Namely, every vertical profile generated by the model at high resolution is used to generate a plane-parallel precipitating environment, to which the RTM is then applied to compute the upwelling TBs that would be measured by the satellite radiometer at an observation angle of 53.1°. [Note that with this assumption, the different spatial resolutions and antenna patterns of the various frequencies don't come into play.]

The required inputs to the RTM are: suitable temperature / moisture profiles and temperature / emissivity of the surface, as well as vertical profiles of liquid/ice water contents (LWC/IWC) of the various hydrometeors - along with their single-scattering properties. Surface temperature and vertical profiles are provided by the UW-NMS simulation. Absorption by atmospheric gases at microwave frequencies are calculated according to the Liebe and Gimmestad (1978) and Liebe (1985) clear-moist air refractivity model that provides a combined water vapour – oxygen volume absorption coefficient.

To accommodate the various surface backgrounds being used for the CDRD retrieval algorithm, a consistent and quantitative means to acquire characteristic surface emissivities (reflectances) for variable satellite view angles and for both horizontal and vertical polarizations is essential. Thus a 9-member surface emissivity module (SEM) has been developed. For a rough ocean (*i.e.*, an ocean surface undergoing above-surface winds) the SEM employs the ocean emissivity model of English and Hewison (1998); see also Schluessel and Luthardt (1991) and Hewison and English (2000). This scheme calculates accurate estimates of open sea emissivity between 10 and 200 GHz for observation angles up to 60 degrees and winds between 0 and 20 m s^{-1}. For non-frozen land emissivities, we have adopted two different surface emissivity models from Hewison (2001),

specifically models for “other forestry” and “bare soil”, which we refer to as “vegetated land cover” and “non-frozen bare soil”, respectively. For frozen surfaces we have adopted six surface emissivity models from Hewison and English (1999) consisting of “frozen bare soil”, “snow-covered forest”, “first year ice”, “compact snow”, “fresh wet snow”, and “deep dry snow” -- noting we have imposed various minor name changes from the originals for the frozen surface cases. We also note that the latter four frozen surfaces may be applied to either ocean or land areas.

The uncertainty in surface emissivity is taken into account within the Bayesian retrieval scheme developed by Mugnai et al. 2001 and Di Michele et al. 2003. This is accomplished by means of an error covariance matrix (see Di Michele et al. 2004), which accounts for T_B sensitivity to parameter uncertainties and approximations used in the forward RTM model (e.g., Tassa et al. 2003, 2004).

The determination of the single scattering properties of the various hydrometeors species would be a straightforward calculation in Mie scattering if only pure water and ice spheres are considered, but can be a major challenge due to the wide variety of sizes, densities, and shapes of natural ice hydrometeors - especially for snowflakes and ice aggregates which are hydrometeors large enough to interact with the radiometer frequencies of interest, but whose shapes are typically in radical departure from spheres. However, whereas the UW-NMS model provides hydrometeor size distributions and densities, information on shape is not available from its microphysical parameterization scheme - which is designed strictly to exchange H_2O mass between vapour and the different species of hydrometeors (under the allowed gas-hydrometeor or hydrometeor-hydrometeor mass transfer schemes) without considering the habits under which the mass transfers take place.

For calculations of the single scattering properties of hydrometeors, various assumptions concerning hydrometeor shape are made, since shape information is not comprehensively provided from the NMS bulk microphysical parameterization scheme. In NMS, cloud droplets and rain drops are considered to be spherical and homogeneous, thus their scattering properties can be calculated based on Mie theory. Graupel hydrometeors are assumed to be spherical and homogeneous with a bulk density (mass / volume of a circumscribing sphere) equal to ρ_g (0.9 g/cm^3). Thus Mie theory can also be used to calculate graupel optical properties using the index of refraction of a homogeneous mixture of air and ice, according to the average dielectric function of Maxwell-Garnett [36].

In NMS, pristine crystals represent recently formed particles and are assumed to have a hexagonal plate habit, and size / density formulations described in Section 2.1. Alternatively, the RMS represents pristine crystals as many different simple ice crystal shapes, from needles to plates, all assumed to have the same D_C of 0.024 cm which results in an associated density of 0.1 g cm^{-3}. In order to calculate their optical properties, the Grenfell and Warren [37] approximation scheme is used (see also [38]). In this approximation, the single-scattering properties of each non-spherical particle are calculated by means of a collection (concentration) of solid ice spheres n_S, all equal in size to one another, with a new equivalent diameter (D_S) determined by the ratio of volume over cross-section area (V / A_{cs}) of the original particle. The V factor is derived from the NMS. To obtain the A_{cs} factor, the following relationship from [39] is used:

$$A_{cs} / (\pi D_c^2/4) = K_0 D_c^k$$

for various shapes of ice particles. For our calculations, K_0 and k are taken as 0.18 cm^{-1} and 0.2707, respectively, as indicated by the aforementioned authors for continental cirrus with mixed habit (noting the circumscribing sphere characteristic diameter D_C must be expressed in cm). The result is that the D_S and n_S of the equivalent spheres is given by:

$$D_s = \frac{\rho_p}{\rho_i} \frac{D_c}{K_0 D_c^{\,k}}$$

$$n_s = \left(\frac{K_0}{1-k}\right)\left(\frac{D_c^{3+k}}{K_0 D_s^3}\right)$$

In the NMS, snow and aggregates are porous, low-density and assumed to have variable - complex shapes. In order to represent snow and aggregates as non-spherical particles, we adopt the approximations developed by Surussavadee (2006), Surussavadee and Staelin (2006, 2008a,b) in which the results of several single scattering simulations of non-spherical particles have been reproduced synthetically using the Mie solution for spheres of equivalent mass and a density formulation $\rho(\nu)$ that is a function of frequency (ν). In this fashion, both radii and densities of the simulated hydrometeors are changed to take into account the optical effect of non-sphericity, without altering their masses. In detail, snow and aggregates are approximated by equal-mass spheres that are mixtures of ice and air having densities $0 < \rho(\nu) < 0.9$ g cm^{-3} that depend on habit and ν. It is important to note that $\rho(\nu)$ is that of an optically-equivalent particle and can be quite different from the density of hard ice, as well as different from the bulk density of the original particle itself. The formulation is:

$$\rho(\nu) = \gamma \cdot 10^{-3} \cdot \nu + \eta$$

where for snow (corresponding to plates), the parameters γ and η are 0.815 g cm^{-3} s^{-1} and 0.012 g cm^{-3}, respectively, while for aggregates (corresponding to 6-arm bullet rosettes) they are 0.863 g cm^{-3} s^{-1} and 0.115 g cm^{-3}, respectively and ν is expressed in GHz.

Once individual absorption, scattering, and asymmetry factors have been calculated for the components hydrometeors of a vertical grid cell, they are integrated over the PSDs to obtain bulk absorption / scattering efficiencies and asymmetry factors for the entire microphysical mixture. This process then continues throughout the vertical extent of the microphysical profile. Next, the boundary emissivities (reflectances) from the surface are obtained from the SEM (see next sub-section). Finally, the multiple scattering RTE model is invoked to obtain the simulated TOA satellite TBs. Because Mie equations are used in calculating the scattering phase functions of equivalent spheres, the RMS's RTE model cannot introduce polarization to the radiation field due to the cloud hydrometeors themselves. However, polarization is introduced through the polarized reflecting surface backgrounds.

3.3 The instrument model

The transfer function of the MW radiometer is required to convert the radiance at the antenna input to brightness temperatures at the instrument output. In the NMS simulations, every pixel is considered homogeneous in terms of meteorological and microphysical characteristics. Real clouds observed by satellite PMW radiometers, with instantaneous-field-of-view (IFOV) resolutions typically ranging from 6 - 60 km (depending on satellite altitude, radiometer antenna size and channel frequency) are typically heterogeneous. In the RMS, an approximation scheme is used to mitigate against incomplete beam filling errors. Once the monochromatic TBs have been calculated at 2-km resolution, they are averaged to the sensor resolution (varying with frequency) using a 2-dimensional Gaussian spread function $P(x,y)$ reproducing the antenna pattern:

$$P(x,y) = \frac{1}{\sqrt{\pi}\sigma_x} e^{-\frac{1}{2}\left(\frac{x-\mu_x}{\sigma_x}\right)} \cdot \frac{1}{\sqrt{\pi}\sigma_y} e^{-\frac{1}{2}\left(\frac{x-\mu_y}{\sigma y}\right)}$$

where μ_x and μ_y are the central IFOV coordinates of a radiometer channel elliptical ground footprint, and the standard deviations of the antenna pattern response functions along the major axis (x) and minor axis (y) directions are given by:

$$\sigma_x = \frac{1}{2\sqrt{2\ln(2)}} IFOV_x$$

$$\sigma_x = \frac{1}{2\sqrt{2\ln(2)}} IFOV_x$$

where $IFOV_X$ and $IFOV_Y$ are the corresponding down-scan (major axis) and cross-track (minor axis) IFOVs, respectively. These procedure thus gives the greatest weight to the central beam regions where quasi-homogeneity can be assumed, and least weight to the outer regions where whatever heterogeneity is present may begin to impose itself.

3.4 Cloud Dynamic Radiation Database

To generate the Cloud Dynamics and Radiation Database (CDRD). for the European region to be used within the H-SAF project, sixty simulations of different precipitation events over the European area for the March 2006 - February 2007 one-year period were performed by means of the cloud resolving model UW-NMS, in such a way as to take into account the various climatic regions, types of precipitation and seasonal variations. Next figure shows their inner domains.

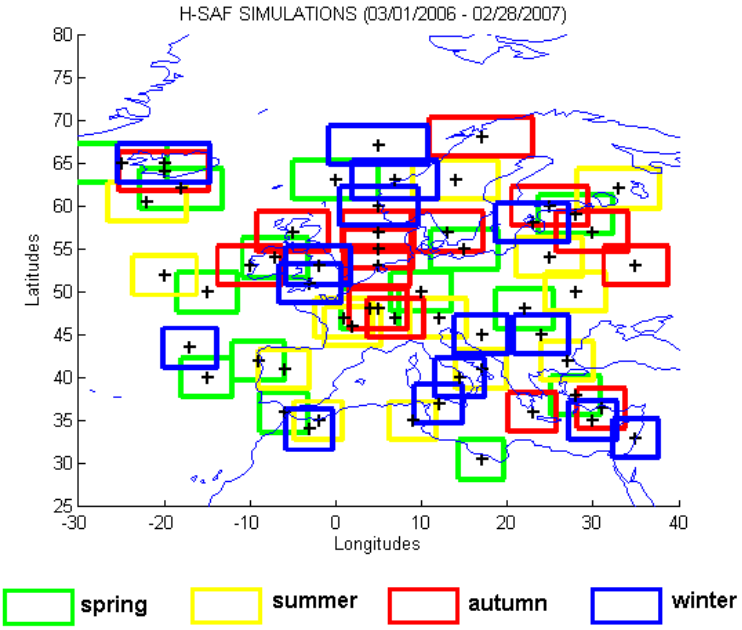

Figure 4 Inner domains of the 60 NMS simulations, divided by season

In essence, we have generated CDRD databases for the European region, that cover one entire year from March 1, 2006 to February 28, 2007 and are divided by seasons and equally distributed over them – specifically, for each season there are 15 simulations that are selected in order to make the database as complete as possible.

For each simulation, three two-way nested grids are configured. The vertical grid extends to 17 km divided into 36 levels with variable, height-dependent grid spacing. The horizontal grid configuration is comprised of: (1) an outer domain of 4,500 x 4,500 km at 50-km resolution, (2) a first interior domain of 900 x 900 km at 10-km resolution, and (3) a second interior and innermost domain of 500 x 500 km at 2-km resolution. Simulation cases are selected to ensure thorough sampling over an

extensive manifold of multi-channel TBs and across a wide range of meteorological and microphysical conditions containing precipitation.

Each simulation was run for 24 or 36 hours with a 12-hour spin-up time. This initial period is necessary to better initialize the model by adapting the initial data to the maximum resolution of the model. The NOAA National Centers for Environmental Prediction (NCEP) Global Forecasting System (GFS) gridded analysis fields at about 100 km resolution were used as initial conditions and to nudge the boundaries of the outer grid every six hours throughout the simulation period. After the first 12 hours, the model extracts hydrometeor profiles over the inner domain C – this is done every hour of the remaining simulation time.

In creating a CDRD database, it is important to recognize that numerous atmospheric profile realizations are calculated for precipitating situations in which a given realization is made up of: (1) 120 meteorological profiles involving different dynamical, thermodynamical and hydrological variables (*i.e.*, DTH variables), (2) six hydrometeor profiles, (3) a set of geophysical factors identifying the type of underlying surface, the topographic height, and three spatiotemporal coordinates (latitude, longitude, month-of-year), and (4) a TB vector covering all relevant cm-mm wavelengths and polarizations essential for linkage to the operative PMW radiometers. The database is then separated into four subsets depending on the surface background, specifically: (1) rough ocean, (2) vegetated land cover, (3) frozen surface (either ocean or land) or (4) mixed coastline (some combination of ocean, land or frozen surfaces). This discrimination is essential when it becomes necessary to take into account the strong dependence of TOA TBs on the surface radiation boundary conditions, especially for the lower atmospheric window frequencies.

In considering the simulation data, it is from the innermost NMS nests (500 x 500 km domains) that meteorological and microphysical profiles, as well as geophysical factors, are selected for possible database entries. The meteorological parameters are extracted from the outer grid at 50 km and resampled to the inner grid resolution. Using the entire set of 60 simulations, approximately 60 million 2-km microphysical profiles with the associated geophysical factors and DTH variables, are obtained. The RMS is applied in order to assign to each of these database entries, the appropriate 2-km resolution simulated TB vectors -- apposite to the PMW radiometer channel frequencies used for retrieval operations. Once generated, the TB vectors are convolved to the spatial resolution of the corresponding SSMIS channels, using a Gaussian filter as described in Section *3.3*. The simulated high resolution *surface rainfall rates (RR_{sur})* with linked microphysical profiles and DTH variables are convolved to the resolution of the SSMIS's high frequency channels (*i.e.*, 12.5 km for 91.7, 150.0 and 183 ± 1,3,7 GHz). Once this process is completed, the averaged profiles are tested for the presence of precipitation, *i.e.*, the presence of non-zero values of RR_{sur}. Some two million database entries are logged into the final CDRD database, each of which contains the influence of at least one 2-km resolution precipitating profile.

Four dynamical/meteorological parameters are used because they have a high impact within the European / Mediterranena basin region. These parameters are referred to as tags, and they are briefly described below, while for a quantitative beavior description of the tags, and significant results on their use in the CDRD precipitation retrieval methodology please refer to our series of recent papers; Sanò et al., 2013, Smith et al., 2013, Casella et al., 2013, Mugnai et al., 2013b. .

ω_{700} - *vertical velocity at 700 hPa* (Pa s^{-1}): The 700 hPa level tends to be within the cloud region where precipitation is formed, that is generally above the cloud base experiencing moisture and/or hydrometeor fluxes producing or growing precipitation hydrometeors. At mid-latitudes, there is a high probability of rainfall in areas with strong upward vertical velocities and sufficient low level vertical moisture flux. Thus, the combined use of this parameter with converging moisture flux near the

surface can often identify areas of precipitation. Care must be taken, however, in that strong downward vertical velocities will occur in regions of intense precipitation, representing, for example, cold downdrafts or Cb outflow boundaries.

$\Phi q_{\Delta 50}$ - *vertical moisture flux at 50 hPa above ground level (AGL)* (g $m^{-2}s^{-1}$): The direction (sign) of vertical moisture flux at 50 hPa AGL is generally indicative of moisture converging or diverging below the cloud region. A convergent, moist boundary layer is generally required for triggering precipitation and in order for convective thunderstorms to initiate and develop, there must be significant moisture convergence at low levels. By the same token, a weakening precipitating system, such as collapsing squall line, will experience a divergent boundary layer.

CAPE - *convective available potential energy* (J kg^{-1}): CAPE is a measure of buoyant thermodynamic energy found in near-surface air parcels with respect to the ambient environment, generally, but not always, created by heat transfer though turbulence from the surface through the atmospheric surface layer into the planetary boundary layer -- which is often, but not always, well mixed. Whereas its name seems to resonate with the notion that this energy will somehow go directly into convection (assuming sufficient buoyancy), this is not necessarily the case, particularly in the tropics and often at mid-latitudes. What is often true, however, that very strong values of CAPE are often associated with precipitation.

$\mathbf{H_{FL}}$ - *freezing level height or 0°C isotherm level* (m): The freezing level height, by itself, does not necessarily correlate with the presence of precipitation. However, when precipitation is present, there can be correlations between its value and the intensity of precipitation, again with the proviso of "not necessarily". Nonetheless, freezing level height has generally been recognized by meteorologists, usually within a regional perspective, as an important parameter in evaluating whether and how precipitation will occur. For example, in stratiform cloud situations, it is an important parameter in determining where it is likely to find liquid water or ice. It can be used as a climatological parameter that together with season, latitude and surface temperature enables categorization of precipitation accumulation (*e.g.*, [51]). Freezing level height has also used in a number of PMW precipitation retrieval algorithms (*e.g.*, [14, 52]) where climatological mean values are needed.

To analyze the database in terms of consistency and completeness a sample of experimental TBs was built collecting data from 1011 SSMIS overpasses. The results of such study are presented in Casella et al. (2013). In this study it is also proofed that the partitioning of the CDRD in terms of the DTH variables associates itself with distinct microphysics profiles. It is then shown that these distinct profiles give rise to similar TB vectors, proving the essential ambiguity of a CRD type algorithm used without meteorological extensions. Finally it is shown that the non-uniqueness problem of the solution is significantly mitigated when the DTH are taken into account in the retrieval process (this important result has also been demonstrated in Sanò et al., 2013). Some of the results of this study are shown in next figures.

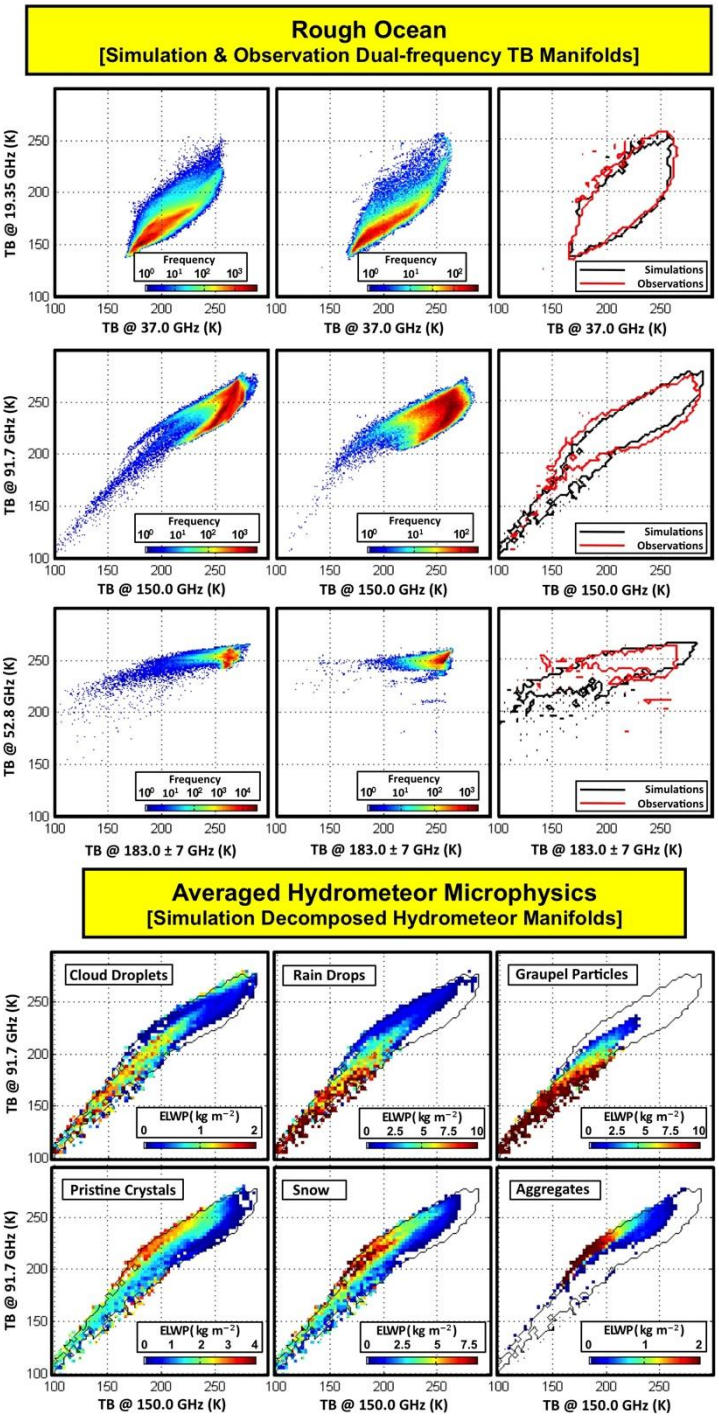

Figure 5 Comparisons of simulation and observation dual-channel-frequency TB manifolds over rough ocean

In figure above:

- Upper three panel rows for three frequency pairings: 19.35 - 37.0 GHz, 91.7 - 150.0 GHz and 52.8 - 183.3 ± 7 GHz.
- Lower two panel rows show corresponding simulation decomposed hydrometeor manifolds associated with 91.7 - 150.0 GHz pairing (see text).
- For upper three rows, left-hand panels consist of simulated manifolds, middle panels consist of

observation manifolds and right-hand panels consist of outer boundaries of both manifolds where color bars are used to indicate absolute frequencies of occurrence based on $\log_{10}$ scale, and for which rough ocean simulation and observation sample sizes are 849 366 and 106 826 entries, respectively.

- For lower two rows, color scales are used to indicate averaged ELWPs in kg m^{-2} for each of six separate hydrometeor species (from Casella et al., 2013)

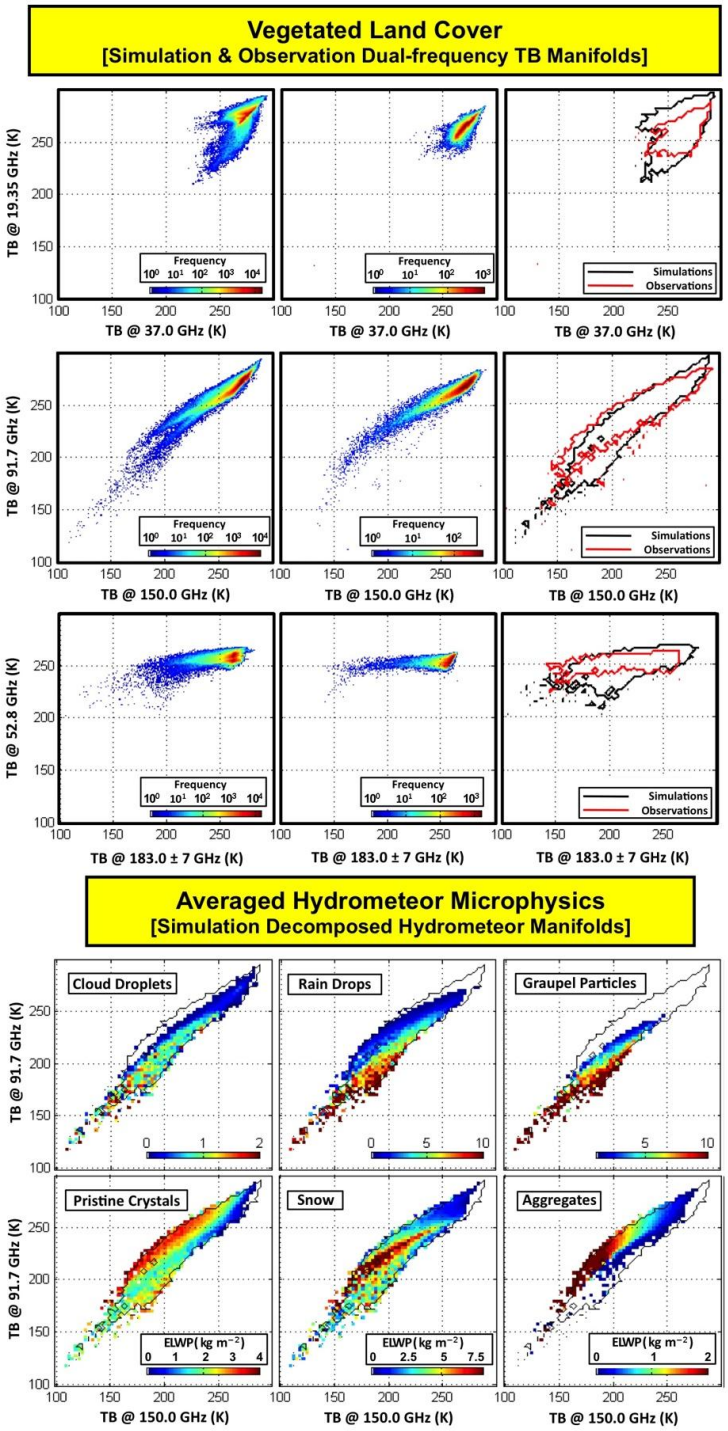

Figure 6 Comparisons of simulation and observation dual-channel-frequency TB manifolds vegetated land cover

In figure above simulation and observation sample sizes are 424 796 and 62 415 entries, respectively (from Casella et al., 2013).

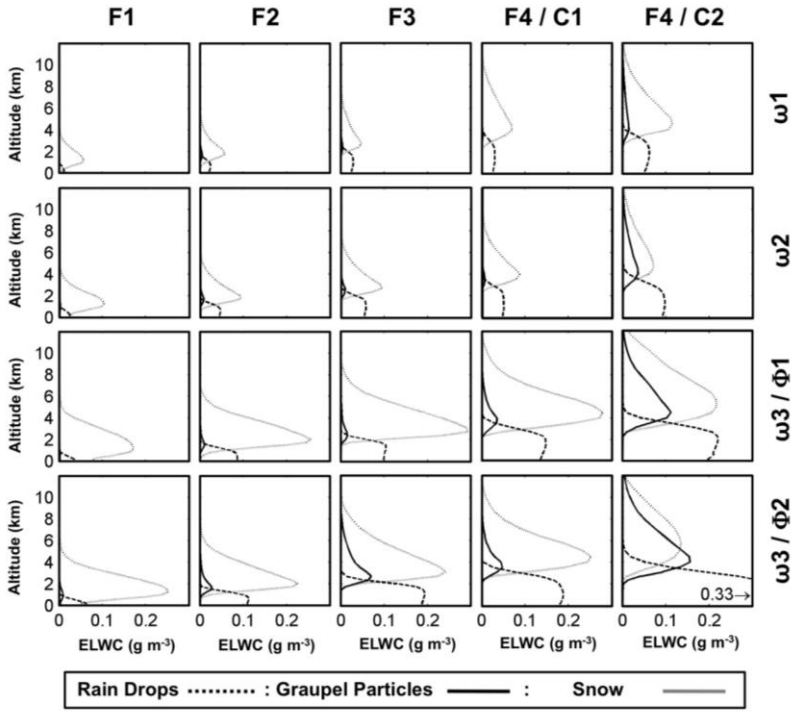

Figure 7 Averaged microphysical profiles from all European / Mediterranean basin database realizations involving three hydrometeor categories (rain drops, graupel particles and snow)

Figure above is based on categorization by four meteorological parameters separated into three ω_{700} categories ω1 to ω3 (from weak to strong mid-level vertical velocity), two $\Phi q_{\Delta 50}$ categories Φ1 & Φ2 (divergent and convergent surface moisture flux), two CAPE categories C1 & C2 (weak-moderate and strong convective available potential energy) and four H_{FL} categories F1 to F4 (from low to high freezing level heights).

Note that only strongest ω_{700} category ω3 (i.e., from 50th to 100th histogram percentile) and highest H_{FL} category H4 (i.e., from 75th to 100th histogram percentile) are subdivided according to Φ1 and Φ2 categories and C1 and C2 categories *(from Casella et al., 2013)*.

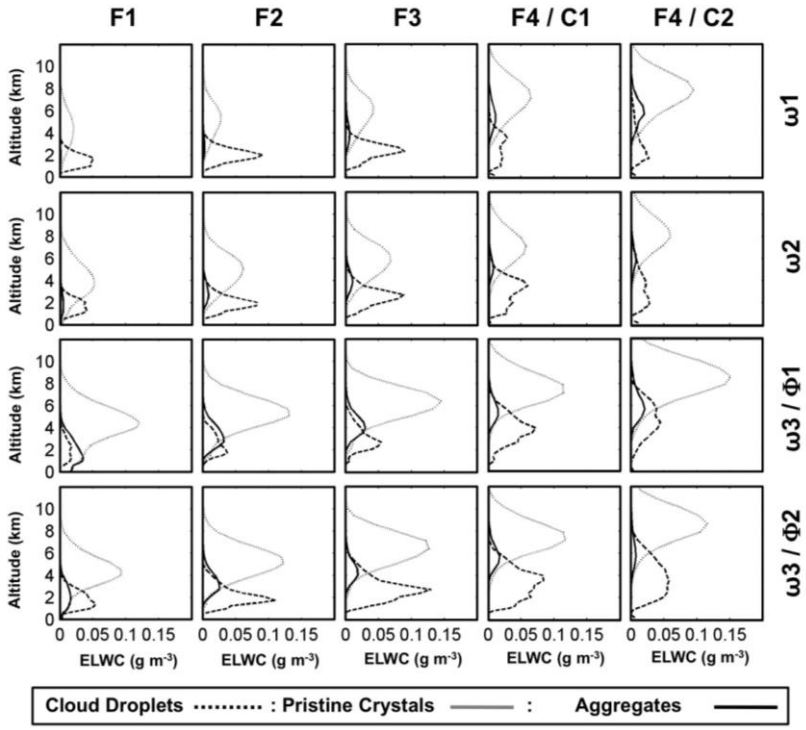

Figure 8 Averaged microphysical profiles from all European / Mediterranean basin database realizations involving three hydrometeor categories (cloud droplets, pristine crystals and aggregates)

3.5 The precipitation retrieval model

As for the retrieval of precipitation, we will use the latest version of a physically-based algorithm for precipitation profile retrieval, that has been developed and is continuously being improved at CNR-ISAC. In the early version, described by Mugnai et al. (1993), Marzano et al. (1994), Pierdicca et al. (1996)(, the solution profiles were derived without iteration by a Bayesian method based on weighing different database profiles according to the proximity of measured and modeled T_B's and on *a priori* probabilities of occurrence of given profile structures. Surface rain rates are derived from the estimated hydrometeor profiles using fallout equations. After Panegrossi et al. (1998), it was evident that precision and accuracy of the precipitating cloud structure estimation, and hence of the surface rainfall rate retrieval, are strictly related to the appropriate generation of the cloud profile dataset associated to the typology of the observed precipitation event more than to an *a-posteriori* statistical treatment of uncertainties. Thus, it is important to use several cloud model simulations for different types of precipitation systems and to generate the corresponding cloud-radiation databases, in order to specialize the algorithm to different storm structures. As a consequence, more recent releases improve the algorithm performance by means of a set of specific simulations to represent meteorological events occurring in the zone and season under investigation. As mentioned before, the simulation of the meteorological events is performed by the UW-NMS.

A former release of the ISAC algorithm has been published with the name of BAMPR (Bayesian Algorithm for Microwave Precipitation Retrieval) - see Mugnai et al. 2001; Di Michele et al. 2003; 2004; Tassa et al. 2003. It is characterized by a detailed description of the estimation uncertainties, a careful coupling of the forward and inverse problem and a quantitative evaluation of the representativeness of the cloud-radiation database. For this project, we have developed a more advanced version of the algorithm – which we call CDRD Algorithm since it is thought to be used within a new approach for passive microwave precipitation retrieval, which we call the Cloud

Dynamics and Radiation Database (CDRD) approach for it is based on extending the CRD method by incorporating an extensive mix of the CRM's dynamical, thermodynamical, hydrometeorological, and microphysical variables. The original idea presented by Mugnai et al. (2006) has been developed within the H-SAF project and described in several recent papers (Sanò et al., 2013, Casella et al., 2012, 2013, Mugnai et al., 2013b, Smith et al., 2013). The main objective in transforming from the CRD to CDRD design has been to reduce non-uniqueness effects that have plagued CRD-type schemes. Such schemes restrict interpretation of observed TBs by ignoring observable dynamical/meteorological/environmanetal information that helps constrain the influence microphysical profile subsets (*i.e.,* the associated hydrometeors, their phases, habits, size distributions and related vertical distributions) that determine the Bayesian retrievals. In the underlying analysis required for developing the CDRD algorithm, we have found convincingly that optimal meteorological variables serve, in a generally quasi-orthogonal fashion with respect to the initial TB-based Bayesian microphysical profile solution subsets, to quarantine candidate profiles which are incongruent with ambient environmental conditions for given observational situations; see Casella et al. (2013). This then serves to mitigate against the ambiguities that would otherwise arise in the solutions.

The block diagram of the CDRD algorithm is shown in next figure, where the two boxes represent the two main blocks of the algorithm, generally referred as the "forward problem" and the "inverse problem". As described earlier, the forward problem consists of the generation of a database (the CDRD), in which the simulated T_B that would be measured by a spaceborne radiometer are associated to the various cloud structures generated by the UW-NMS cloud-resolving model. The frequency-dependent model and instrumental errors are evaluated by means of the error covariance estimator module by using ancillary information and numerical sensitivity tests. The output of the forward modelling procedure is the construction of a statistically significant CDRD.

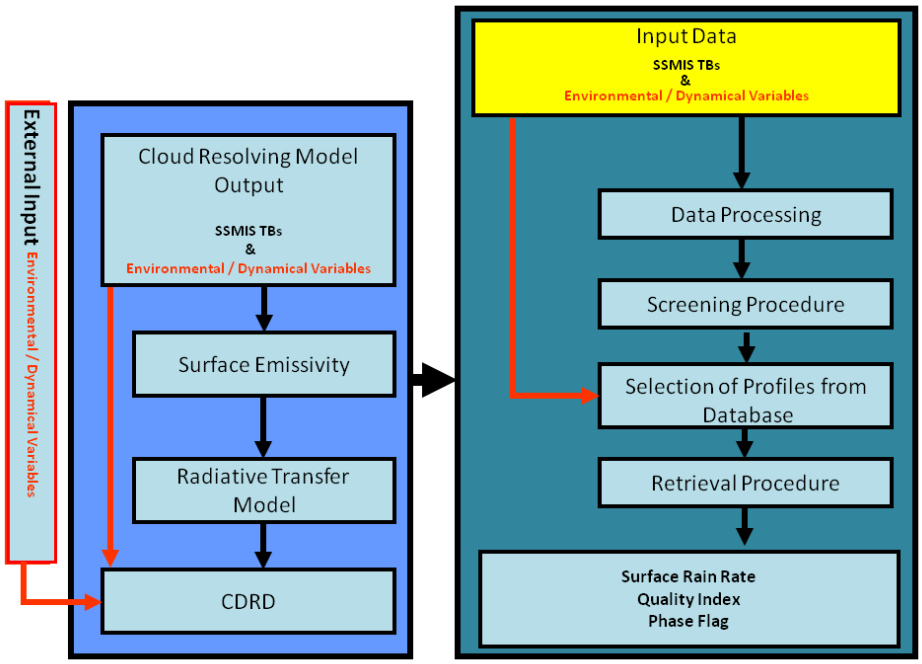

Figure 9 Block diagram of the CDRD Bayesian Algorithm for precipitation profile retrieval

The box on the right represents the “inverse problem”; the box on the left corresponds to the database generation.
Detailed block diagram is here depicted:

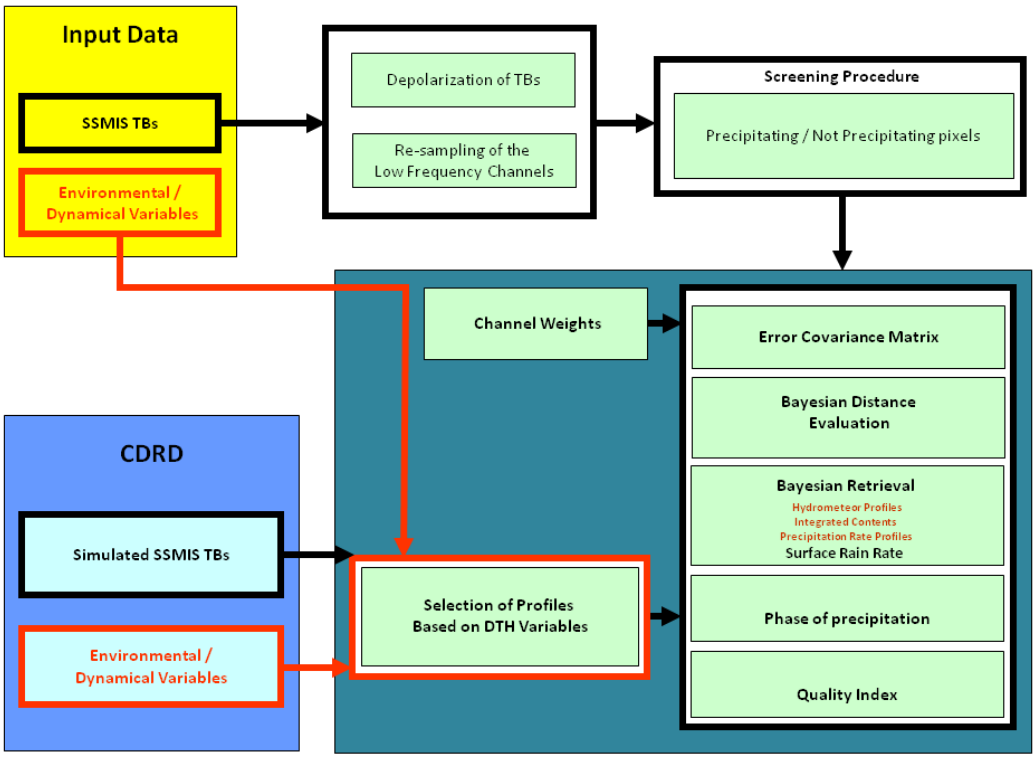

Figure 10 Detailed block diagram of the “inverse problem

The inverse problem consists in retrieving the hydrometeor profiles by means of a Bayesian method that compares the measured (SSMIS) and modeled (CDRD) T_B's. Figure shows the flowchart of our CDRD Bayesian Algorithm. The modifications and improvements of the CDRD methodology over the CRD-type methodology arise by combining meteorological parameter constraints derived from synthetic dynamical-thermodynamical-hydrological (DTH) meteorological profile variables, together with concomitant multi-hydrometeor microphysical profiles and multispectral PMW brightness temperature (TB) vectors into a specialized *a priori* knowledge database underpinning and guiding the algorithm's Bayesian retrieval solver. In the CDRD the meteorological-microphysical knowledge variables are produced by the UW-NMS simulations described above, whereas for the obervations they are derived from ECMWF operational forecast and/or analysis at 0.25 degree resolution, and they are associated to the observed SSMIS TBs.

The new version of the CDRD algorithm developed for PR-OBS-1 consists of four main steps:

1) First, the measured T_Bs at the various channels are processed so as to enhance their resolution up to that of the 89 GHz channels. Secondly, all pixels with unrealistic T_B's are discarded ($T_B < 50$ K & $T_B > 325$ K). A screening procedure is applied in order to identify the regions/pixels where precipitation is unlikely or precipitation retrieval would be ambiguous. Such regions/pixels are not considered by the retrieval algorithm. Different screening procedures have been developed depending on the characteristics of the surface background. The overall procedure for the current screening scheme was originally separated into two parts according to available channels for a given radiometer. The first part is for the conically scanning radiometers which have a set of relatively low channel frequencies between ~18 GHz and ~95 GHz (such as SSM/I). The second part is for the radiometers which have a set of relatively high channel frequencies between ~150 GHz and ~183 GHz, in which at least two of the frequencies around 183 GHz are separated by at least 2,000 MHz. This applies only to the SSMIS radiometer. Since the PR-OBS-1 (ver. 1.7) processes only SSMIS data, the second part only is used in the version of the algorithm developed for H-SAF. The high-end frequency screening procedure follows the algorithm of Chen and Staelin (2003) which they developed for the AMSU-A and AMSU-B/MHS radiometers. For PR-OBS-1, this procedure is adapted for applications with the SSMIS radiometer, but it is coherent to the screening procedure used for the PR-OBS-2 product. The adaptation process requires taking into account differences in IFOV scales and polarizations of the 53.6H GHz, 183±3H and 183±7H GHz channels related to differences between the designs of the SSMIS and AMSU-A/MHS instruments. These differences are addressed by calibrating the SSMIS observed brightness temperatures for the channels involved in the screening procedure to the AMSU observed brightness temperatures. The Chen and Staelin (2003) screening procedure consists in a series of tests on the 53.6H GHz, 183±3H and 183±7H GHz channels. To start, any $TB_{183\pm7H}$ less than the threshold:

has its associated microphysical information packet flagged as potentially precipitating, where in the threshold expression, $TB^{max}_{53.6H}$ is the spatially filtered 53.6H GHz TB obtained by selecting the warmest TB within a 7x7 centered array for a given measurement. Then for a second test, if $TB_{53.6H}$ itself at any given pixel is less than 248K, the information packet is flagged as potentially precipitating if a second near 183H GHz channel frequency, $TB_{183\pm3H}$, is less than another threshold:

For these latter screening conditions, it is assumed that a given observed scene corresponds to a very dry and cold atmosphere, and the $TB_{183\pm7H}$ value might possibly be degraded by contamination from surface emissivity. As a third test, if the $TB_{53.6H}$ is less than 242K, then the measurement is taken as not precipitating.
For SSMIS the screening procedure has been modified in the following way:

a. $TB^{max}_{53.6H}$ and $TB_{53.6H}$ are changed into the warmest TB within a 7x7 centered array for a given measurement of the calibrated 52.3H GHz SSMIS channel, and it will be referred to as $TB^{max}_{52.3H}$. The selection of the SSMIS 52.3H GHz channel is based on the evidence that from a direct comparison of concurrent (near in space and close in time within less than 30 minutes) SSMIS and AMSU-A observations, it showed the best linear correlation with the AMSU-A 53.6H GHz channel. The calibration function used to obtain the SSMIS TB corresponding to the 53.6H GHz TB of AMUS-A is:

   A squared mean difference of less than 1 K^2 between the AMSU 53.6 GHz channel and the result of the calibration has been found.

b. Small biases between the near 183H GHz channel frequencies have been corrected by adding 3 K to the SSMIS brightness temperatures.

2) The second step consists of the actual use of the DTH variables, as a meteorological/environmental constraint to select a portion of the CDRD that in terms of dynamical, meteorological and environmental conditions is more representative of the observed area. PR-OBS-1 in its actual version make use of thermo-dynamical information from ECMWF model. The specific meteorological parameters needed for this study are described in Casella et al (2013). The actual ECMWF data needed to produce these parameters consist of the ongoing optimal initial analyses made every six hours (*i.e.*, t0 times) and at 3-hour forecast times. These time coordinates ensure that no linearly-interpolated meteorological estimate aligned exactly to a satellite overpass time is out of phase by more than 90 minutes. The required meteorological parameters are extracted from forecast results on a regularly spaced latitude-longitude grid at 50 km resolution.

3) In the third phase, the Bayesian Minimum Mean Square (MMS) inversion algorithm is applied using only the class of profiles of the CDRD selected according to consistency of the ECMWF derived DTH variables associated to the observations, and the DTH variables in the CDRD. Output products can be the hydrometeor and/or precipitation rate profiles, columnar liquid water contents and surface rain rates. Within the MMS Bayesian criterion, the hydrometeor profile estimate is given by the expected value of the hydrometeor profile conditioned to the space borne measured multi-frequency T_B, i.e. it is practically an ensamble weighed average of the hydrometeor profiles (belonging to the selected CDRD) whose radiative signature lie around the observed T_B. The MMS approach helps in overcoming some stability problems due to the numerical implementation of the Maximum A-posteriori Probability (MAP) algorithm (Marzano et al. 1999).

If we indicate with **g** the geophysical (hydrometeor water content) vector related to a profile set of the CRD and with $\mathbf{t_m}$ the multi-spectral vector of the simulated brightness temperatures, the MMS estimate $\hat{g}_{MMS}$ is defined as the expected value of **g**, given a set of measurements $\mathbf{t_m}$, i.e.

$$\hat{g}_{MMS} = \langle \mathbf{g} \mid t_m \rangle$$

where the angle brackets indicate an ensamble averaging with respect to **g**. The previous equation can be given in an explicit form as

$$\hat{g}_{MMS} = \int_0^\infty g p(g \mid t_m) dg$$

where p(**g**|**t**$_m$) is the conditional probability density function (PDF) of **g**. Using the Bayes theorem, p(**g**|**t**$_m$) can be transformed in the following way:

$$p(g \mid t_m) = p(t_m \mid g) p(g) / p(t_m) = p[\varepsilon_t(g)] p(g) / p(t_m)$$

where the p(**g**) is the a priori PDF due to **g**, and ε_t(**g**)=[**t**(**g**)-**t**$_m$] is the T_B error vector with **t**(**g**) the simulated vector, related to **g** through the radiative transfer model.

The implementation of the last equation can be carried out by noting that, since the CRD consist of a discrete number of profiles (N_{CRD}), the available PDFs are not continuous functions, unless we choose analytical expressions. The PDF p(**g**) for each profile may be approximated as

p(**g**) ~ h(**g**,**Δg**),

where h(**g**,**Δg**) is the histogram relative to the sample **g** within a variable bin **Δg**. Thus, the *i*-th element **g**(*i*) of the hydrometeor profile g can be estimated as follows:

$$\hat{g}_{MMS}(i) = k \sum_{j=1}^{N_{CRD}} g_j(i) e^{-0.5(t(g_j)-t_m)^T C_{\varepsilon_t}^{-1}(t(g_j)-t_m)} h(g_j(i), \Delta g_j)$$

where $\mathbf{g}_j$ is the *j*-th sample of the CRD, **t**($\mathbf{g}_j$) is the corresponding T_B, and $C_{\varepsilon t}$ is the error covariance matrix. The constant *k* is such that:

$$\sum_{j=1}^{N_{CRD}} e^{-0.5(t(g_j)-t_m)^T C_{\varepsilon_t}^{-1}(t(g_j)-t_m)} h(g_j(i), \Delta g_j) = 1.$$

The strong non-linearity of the forward problem implies a non-uniqueness feature of the inverse problem so that very different microphysical structures can produce similar T_B vectors. A remarkable feature of the Bayesian retrieval approach is that each estimate is accompanied by its relative uncertainty (i.e., Marzano et al. 2000, Bauer 2001, Sanò et al., 2013). The Minimum Mean Square (MMS) algorithm, described in the previous Section, can provide a measure of this inherent uncertainty according to equation

$$\sigma^2_{gMMS} = \left\langle [(g \mid t_m) - \hat{g}_{MMS}]^2 \right\rangle$$

where σ^2_{gMMS} is the variance vector of the estimated profile $\hat{g}_{MMS}$. The amount of this uncertainty depends on the capability of the cloud radiative model simulation to reproduce the spatial structure and the dynamical range of the upwelling radiation as well as on the typology of the meteorological event observed. As it has been shown in Tassa et al. 2003, the impact of the uncertainties is extremely large at light rainfall rates (below 2 mm/h), and it tends to rapidly decrease for increasing rain rates. This is probably due both the instruct limitation of passive microwave measurements in

detecting light rain over land, and also to the fact that the events studied in that case were tropical hurricanes and storms, where the presence of light rainfall rate is not well stressed out.

It is worth noticing that the database classification based on the DTH variables plays an important role in this regard as it reduces the inherent dispersion of cloud profiles associated to a given T_B vector. The importance of the representativeness has been stressed. For this reason for H-SAF the CDRD has been developed with a great effort in simulating different events especially over northern Europe and the Mediterranean Sea. In this way, the precipitation database over Europe is represented by the mid-to-high latitude type of events. It is worth noting, however, that the limitation in screening light precipitation and/or snow over vegetated land or over a frozen background still remains one of the main weaknesses in passive microwave precipitation retrieval. The improved representativeness of the database alone will not solve this issue, at least until the next generation of PMW radiometers are in space during the GPM era, can we expect significant progress to be made on this problem.

3.6 Quality Index and phase flag

In the last step of the PR-OBS-1 product generation chain, a pixel based quality flag and a pixel based phase flag is computed.

Quality index

The quality flag summarizes the product quality and reliability and provides the end-users with a simple and immediate criterion for the evaluation of the products towards a correct selection and application of the precipitation estimates with respect to the analyzed scenario.

This index is derived from the "Percentage of Confidence Index" (PCI), evaluated on the base of four different criteria:

1) ***Quality of input data*** (used sensor, type and number of channels used, horizontal resolution, malfunctioning of radiometers);
2) ***Background surface index*** (type of surface, snowy background, presence of ice);
3) ***Event type index*** (snow storm, stratiform rain, convective cells);
4) ***Internal algorithm performance index*** (Bayesian variance of the retrieval for PR-OBS-1).

The quality index and the PCI are connected as shown in the following table:

Percentage of confidence index	Quality flag	Quality index
0	Missing data	0
1-20	Poor	1
21-80	Fair	2
81-100	Good	3

Table 1: Quality index values and interpretation and correspondence with percentage of confidence index (PCI).

The PCI evaluation procedure is based on the following steps:

1. The output of the screening procedure is considered. For pixels without presence of rain a preliminary value of PCI is evaluated according to some conditions on the $TB^{max}_{52.3H}$ (defined in the screening module, see Section 4.5).
2.

Test on TB	Environmental situation	Preliminary PCI
$TB^{max}_{52.3H}$ < 242 K	very cold/dry (not precipitating)	0
$TB^{max}_{52.3H}$ >=242 K & $TB^{max}_{52.3H}$ < 248 K	cold/dry situation	20
$TB^{max}_{52.3H}$ >= 248 K	warm/wet situation	50

Table 2: Preliminary PCI thresholds based on screening algorithm.

3. The presence of snow/ice on areas without precipitation lowers the value of the PCI (the PCI value is limited to 10).
4. For rainy pixels the PCI value is based on a procedure that identifies the event typology. This procedure (Funatsu 2007, 2012) classifies the event in not identified/light stratiform, stratiform, convective, heavy convective (overshooting top) and associates a preliminary value of PCI according to the following table.

Typology of event	Preliminary PCI
not identified/light stratiform	40
stratiform	50
convective	90
heavy convective	90

Table 3: Preliminary PCI based on precipitation type

5. The presence of snow/ice on area with precipitation lowers the value of the PCI (the PCI value is limited to 10).
6. The PCI value associated to precipitation on coastal area is limited to 30 ("fair").
7. The preliminary PCI value is combined to some correction coefficients to become the final value of PCI:
   - satellite operation status coefficient (the PCI value decreases when satellite has some problem, i.e.. damaged channels, etc);
   - not reliable data coefficient (the PCI is set to 0 in case of unrealistic value of measured TB's);
8. The preliminary PCI is then modified according to an internal algorithm performance index based on the relative Bayesian variance.

Phase flag

The phase flag is based on the studies on snow and ice detection of Surussavadee and Staelin (2009) and Rosencrantz (2003). In these studies snowfall is detected by the use of TBs at 20.3 GHz, 50.3 GHz and 89 GHz , and on combinations of these channels. The phase identification procedure compares the selected TBs and their derived quantity with some thresholds to distinguish between liquid or iced precipitation, and to be able to detect falling snow over snowy or iced background. The thresholds are based on the use of AMSU-A and AMSU-B/MHS channels, and these same thresholds are used for PR-OBS-1 (ver. 1.7) and PR-OBS-2 (ver. 2.4).

With reference to Grody et al. (2000), the following indices are used to identify the presence of snowy and iced background:

TT	=	$168+0.49\ TB_{89}$	(over land)
Scattering index	=	$TB_{23}-TB_{89}$	(over land)
Discriminate function	=	$5.1+0.078\ TB_{23}-0.096\ TB_{50}$	(over ocean)

The phase flag is evaluated only for pixels flagged as precipitating after the screening procedure and it is not available over coastal background surfaces.
The phase flag is given as an integer number according to the code table of the standard output field associated. The integers will be associated as follows:

Phase flag	Integer value
unknown (flag determination not reliable)	0
Liquid	1
Ice	2
Mixed	3
missing value (bad data, or precipitation retrieval not available)	7

Table 4: Phase flag values and interpretation

The following figure shows an example of phase flag for a case study over Italy (10/02/2012) when extensive snowfall affected the Central regions of the peninsula.

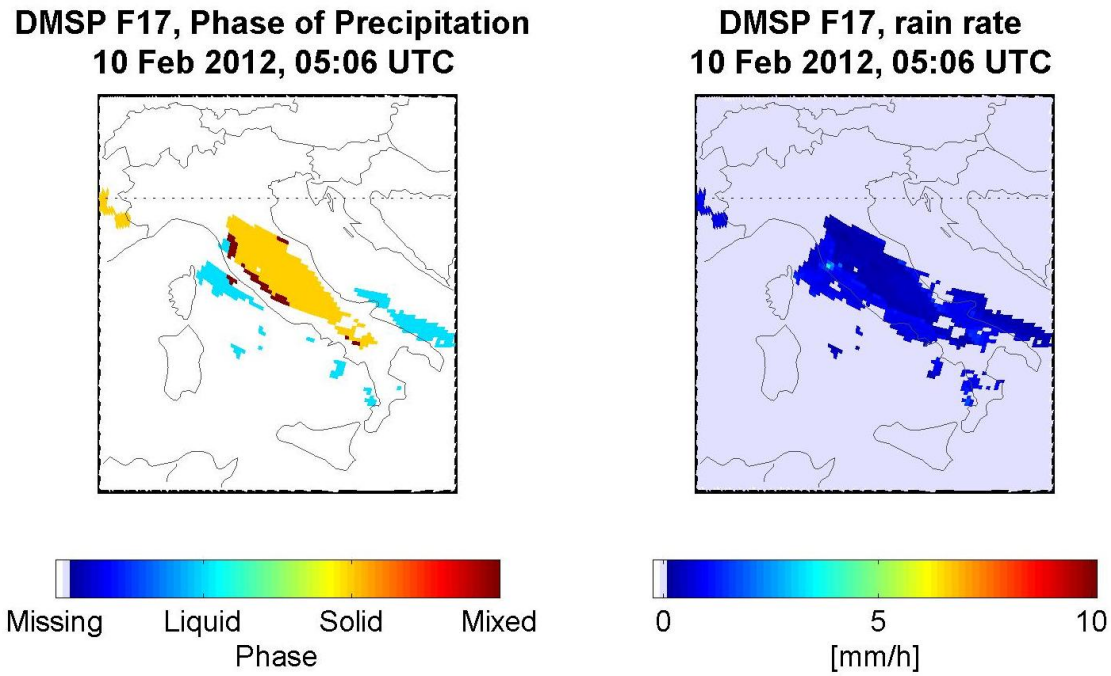

Figure 11 Example of phase flag for PR-OBS-1 ver. 1.7

In figure above: Left: Phase of precipitation; right retrieved precipitation [mm/h]; - Satellite DMSP-F17,SSMIS, day 10/02/2012 05:06 UTC (snow event in Central Italy).

3.7 Algorithms validation/heritage

The physical foundations of the Cloud Radiation Database (CRD) approach were defined in the early 90's by Mugnai et al. 1990, 1993 and Smith et al. 1992, 1994a. At about the same time, multifrequency inversion-type precipitation-profile retrieval schemes based on such approach began to evolve (see Smith et al. 1994b; Kummerow and Giglio 1994a, 1994b; Marzano et al. 1994) and to

successfully participate in algorithm validation/intercomparison activities, such as the First and Second WetNet Precipitation Intercomparison Project (PIP-1 and PIP-2) (see Barrett 1994, Smith et al., 2002). Soon after it became evident that Bayesian retrieval techniques were best suited for the CRD approach (see Evans et al. 1995; Pierdicca et al. 1996). Nevertheless, it was with the launch of the Tropical Rainfall Measuring Mission (TRMM) space observatory in November 1997, carrying onboard the TRMM Microwave Imager (TMI) and a Precipitation Radar (PR), that such physically-based Bayesian techniques were fully exploited and showed their potential for retrieving tropical precipitation – in addition to our BAMPR algorithm, we must mention here the Goddard Profiling Algorithm (GPROF) (Kummerow et al. 2001), evolved into the current version of the TRMM facility algorithm described in Kummerow et al., 2011, Munchak and Kummerow, 2011), which is NASA's official algorithm for TMI retrievals. Thereafter, the optimized algorithms for TMI have been adapted for retrieving precipitation at higher latitudes using SSM/I and SSMIS observations.

The new version of PR-OBS-1 (ver 1.7) has been found to perform reasonably well over sea and vegetated land for all types of precipitation as evaluated against radar and raingauge data. The algorithms also work over land with snow and sea ice, but with a strong risk of false detections. The major improvements of this new version with respect to the former versions is the increased horizontal resolution of the surface precipitation rate (12.5 km vs. 30 km), the consistency of the precipitation estimates and screening with PR-OBS-2 (ver. 2.4), and the retrieval of the phase of the precipitation. Another major improvement, which will have substantial effects on the validation results, is the determination of a pixel based quality index to be associated to the precipitation retrieval.

4 Examples of PR-OBS-1 products

Fig. 11 Fig. 12 and ***Fig. 13*** show precipitation maps associated to a heavy rain event, to a moderate perturbation and to a snow situation, respectively.

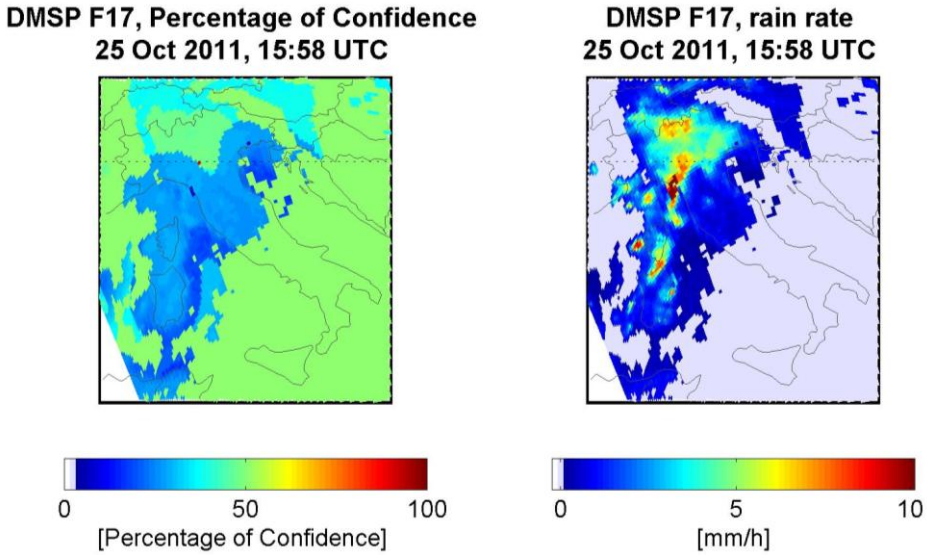

Figure 12 Example of an intensive convective event over northern Italy

The strong convective system (figure above) caused the Genoa city flood during the 25th October 2010 - Left: Percentage of confidence of retrieval; right retrieved precipitation [mm/h]; - Satellite DMSP-F17,SSMIS, day 25/20/2010 15:58UTC, ascending pass.

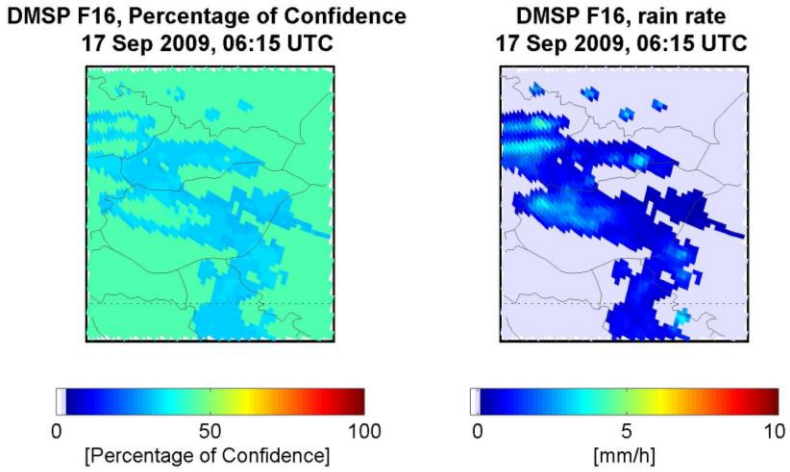

Figure 13 Example of moderate perturbation over Hungary

In figure above: Left: Percentage of confidence; right retrieved precipitation [mm/h]; - Satellite DMSP-F16, SSMIS, day 19/09/2009 06:15 UTC, ascending pass.

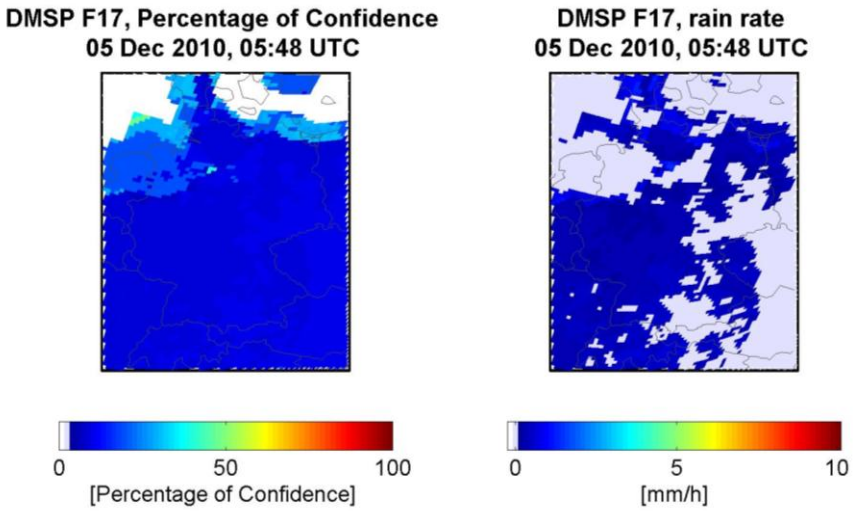

Figure 14 Example of snowfall over Germany

In figure above: Left: Percentage of confidence; right retrieved precipitation [mm/h]; - Satellite DMSP-F17, SSMIS, day 05/12/2010 05:48 UTC, descending pass.

5 References

Barrett E.C. (Ed.), 1994: "The First WetNet Precipitation Intercomparison Project (PIP-1)". Special Edition, *Remote Sens. Rev.*, 11, 423 pp.

Bauer P., 2001: "Over-ocean rainfall retrieval from multi-sensor data of the Tropical Rainfall Measuring Mission (TRMM). Part I: Development of inversion databases". *J. Ocean. Atmos. Tech.*, **18**, 1315–1330, 2001.

Bauer P., L. Schanz and L. Roberti, 1998: "Correction of the three-dimensional effects for passive microwave remote sensing of convective clouds". *J. Appl. Meteor.*, **37**, 1619-1632.

Bauer, P., E. Moreau, F. Chevallier, and U. O'Keeffe, "Multiple-scattering microwave radiative transfer for data assimilation applications," *Q. J. Roy. Meteor. Soc.,* vol. 132, pp. 1259-1281, Apr 2006.

Bohren C.F. and D.R. Huffman, 1983: "*Absorption and Scattering of Light by Small Particles*". John Wiley & Sons, 530 pp.

Casella, D., Dietrich, S., Formenton, M., Mugnai, A., Panegrossi, G., Sanò, P., Smith, E.A., and Tripoli, G.J: Verification of Cloud Dynamics and Radiation Database (CDRD) passive microwave precipitation retrieval algorithm using TRMM satellite radar and radiometer measurements over southern Mediterranean basin, in: Extended Abstract Volume of the 12th Specialist Meeting on Microwave Radiometry and Remote Sensing of the Environment, Rome, Italy, 5-9 March 2012, 4 pp., 2012.

Casella, D., Panegrossi, G., Sanò, P., Mugnai, A., Smith, E.A., Tripoli, G.J., Dietrich, S., Formenton, M., Di Paola, F., Leung, H. W.-Y., and Mehta, A.V.: Transitioning from CRD to CDRD in Bayesian retrieval of rainfall from satellite passive microwave measurements, Part 2: Overcoming database profile selection ambiguity by consideration of meteorological control on microphysics, *IEEE Trans. Geosci. Remote Sens*., in press, 2013

Chen, F.W., and Staelin, D.H.: AIRS/AMSU/HSB precipitation estimates, *IEEE Trans. Geosci. Remote Sens*., 41, 410-417, 2003

Cotton W.R., G.J. Tripoli, R.M. Rauber and E.A. Mulvihill, 1986: "Numerical Simulation of the effects of varying ice crystal nucleation rate and aggregation processes on orographic snowfall". *J. Clim. Apl. Meteor.* **25:** 1658-1680.

Cotton W.R., M.A. Stephens, T. Nehrkorn and G.J. Tripoli, 1982: "The Colorado State University three-dimensional cloud / mesoscale model-1982. Part II: An ice phase parameterization". *J. Rech. Atmos.* **16:** 295-320.

Di Michele S., F.S. Marzano, A. Mugnai, A. Tassa and J.P.V. Poiares Baptista, 2003: "Physically-based statistical integration of TRMM microwave measurements for precipitation profiling". *Radio Sci*., **38**, 8072-8088.

Di Michele S., F.S. Marzano, A. Mugnai, A. Tassa, P. Bauer and J.P.V. Poiares Baptista, 2004: "The Bayesian algorithm for microwave-based precipitation retrieval (BAMPR): Description and application to TMI data". *IEEE Trans. Geosci Remote Sens.*, in press.

English S. and T.J. Hewison, 1998: "A fast generic millimetre wave emissivity model". *Proc. SPIE on Microwave Remote Sensing of the Atmosphere and Enviroment*, 22-30.

Evans K.F., J. Turk, T. Wong and G.L. Stephens, 1995: "A Bayesian approach to microwave precipitation profile retrieval**"**. *J. Appl. Meteor.*, **34**, 260–279.

Funatsu, B. M., V. Dubreuil, C. Claud, D. Arvor, and M. A. Gan (2012), Convective activity in Mato Grosso state (Brazil) from microwave satellite observations: Comparisons between AMSU and TRMM data sets, J. Geophys. Res., 117, D16109, doi:10.1029/2011JD017259.

Funatsu, B. M., C. Claud, and J.-P. Chaboureau (2007), Potential of Advanced Microwave Sounding Unit to identify precipitating systems and associated upper-level features in the Mediterranean region: Case studies, J. Geophys. Res., 112, D17113, doi:10.1029/2006JD008297.

Flatau P., G.J. Tripoli, J. Berlinde and W. Cotton, 1989: "The CSU RAMS Cloud Microphysics Module: General Theory and Code Documentation". *Technical Report 451*, Colorado State University, 88 pp.

Grenfell T.C. and S.G. Warren, 1999: "Representation of a nonspherical ice particle by a collection of independent spheres for scattering and absorption of radiation". *J. Geophys. Res.*, **104**, 31697-31709.

Groody N., F. Weng and R. Ferraro, Application of AMSU for obtaining hydrological parameters, Microwave Radiometry and Remote Sensing of the Earth's Surface and Atmosphere, P. Pampaloni, S. Paloscia , eds.: VSP, 2000. pp.339-352.

Hewison T.J., 2001: "Airborne measurements of forest and agricultural land surface emissivity at millimeter wavelengths". *Geoscience and Remote Sensing*, IEEE Transactions, vol. 39, issue 2, 393-400.

Hewison T.J. and S.J. English, 1999: "Airborne retrievals of snow and ice surface emissivity at millimeter wavelengths". *Geoscience and Remote Sensing*, IEEE Transactions. vol. 37, issue 4, 1871-1879.

Hewison, T. and S. English, 2000: "Fast models for land surface emissivity". In *Radiative Transfer Models for Microwave Radiometry* (C. Matzler, ed.), COST Action 712, Directorate-General for Research, European Commission, Brussels, Belgium, 117-127.

Heymsfield A.J. and L.M. Miloshevich, 2003: "Parameterizations for the cross-sectional area and extinction of cirrus and stratiform ice cloud particles". *J. Atmos. Sci.*, **60**, 936-956.

Kidd C., 1998: "On rainfall retrieval using polarization-corrected temperatures". *International Journal of Remote Sensing*. Vol.19, No.5, 981-996

Kulie, M. S., R. Bennartz, T. J. Greenwald, Y. Chen, and F. Z. Weng, "Uncertainties in Microwave Properties of Frozen Precipitation Implications for Remote Sensing and Data Assimilation," *J. Atmos. Sci.,* vol. 67, pp. 3471-3487, Nov 2010.

Kummerow C. and L. Giglio, 1994a: "A passive microwave technique for estimating rainfall and vertical structure information from space. Part I: Algorithm description". *J. Appl. Meteor.*, **33**, 3-18.

Kummerow C. and L. Giglio, 1994b: "A passive microwave technique for estimating rainfall and vertical structure information from space. Part II: Applications to SSM/I data". *J. Appl. Meteor.*, **33**, 19-34.

Kummerow C.D., Y. Hong, W.S. Olson, S. Yang, R.F. Adler, J. McCollum, R. Ferraro, G. Petty, D.-B. Shin and T.T. Wilheit, 2001: "The evolution of the Goddard Profiling Algorithm (GPROF) for rainfall estimation from passive microwave sensors". *J. Appl. Meteor.*, **40**, 1801-1820.

Kummerow, C.D., Ringerud, S., Crook, J., Randel, D., and Berg, W.: An observationally generated *a priori* database for microwave rainfall retrievals, J. Atmos. Oceanic Technol., 28, 113-130, 2011

Liebe H.J. and G.G. Gimmestad, 1978: "Calculation of clear air EHF refractivity". *Radio Sci.*, **13**, 245-251.

Liebe H.J., 1985: "An updated model for millimeter wave propagation in moist air". *Radio Sci.*, **20**, 1069-1089.

Liou, K., *An Introduction to Atmospheric Radiation (2nd Edition)* vol. 84: Academic Press, 2002.

Liu Q., C. Simmer and E. Ruprecht, 1996: "Three-dimensional radiative transfer effects of clouds in the microwave spectral range". *J. Geophys. Res.*, **101**, 4289-4298.

Macklin, W. C.: "The density and structure of ice formed by accretion," *Q. J. Roy. Meteor. Soc.,* vol. 88, pp. 30-50, 1962.

Marzano F.S., A. Mugnai, E.A. Smith, X. Xiang, J.E. Turk and J. Vivekanandan, 1994: "Active and passive remote sensing of precipitation storms during CaPE. Part II: Intercomparison of precipitation retrievals from AMPR radiometer and CP-2 radar". *Meteor. Atmos. Phys.*, 54: 29-52.

Marzano F.S., A. Mugnai, G. Panegrossi, N. Pierdicca, E.A. Smith and J. Turk, 1999: "Bayesian estimation of precipitative cloud parameters from combined measurements of spaceborne radiometer and radar". *IEEE TRans. Geosci. Remote Sens.*, 37: 596-613.

Marzano F.S., S. Di Michele, A. Tassa and A. Mugnai, 2000: "Bayesian techniques for precipitation profiles retrieval from spaceborne microwave radiometers". In *Proceedings of PORSEC-2000*, pp.221-228, Indian Natl. Inst. Of Oceanogr., Goa, India.

Mugnai A., D. Casella, M. Formenton, P.Sanò, G.J. Tripoli, W.Y. Leung, E.A. Smith and A. Metha, 2009: "Visiting Scientist Activity in Support of WP 2400,VS 310 Programme Activity Report - Generation of an European Cloud-Radiation Database to be used for PR-OBS-1 (Precipitation Rate at Ground by MW Conical Scanners) – *ftp.meteam.it/hsaf/Visiting-Scientist/VS-approved/VS-310-ITALY/ H-SAF_vs310-VS_GT-HL_Final-Report.pdf*.

Mugnai A., E.A. Smith and G.J. Tripoli, 1993: "Foundations for statistical-physical precipitation retrieval from passive microwave satellite measurements. Part II: Emission source and generalized weighting function properties of a time dependent cloud-radiation model". *J. Appl. Meteor.*, 32: 17-39.

Mugnai A., F. Baordo, J. Hoch, C.M. Medaglia, A. Metha, E.A. Smith and G.J. Tripoli, 2006: "Precipitation retrieval and analysis of severe storm events based on Cloud Dynamics and Radiation Database (CDRD) approach". *Geophysical Research Abstracts*, Volume 8, ISSN:1029-7006, EGU General Assembly 2006, Vienna, Austria, 2-7 April 2006.

Mugnai A., H.J. Cooper, E.A. Smith and G.J. Tripoli, 1990: "Simulation of microwave brightness temperatures of an evolving hail storm at SSM/I frequencies". *Bull. Amer. Meteor. Soc.*, **71**, 2-13.

Mugnai A., S. Di Michele, F.S. Marzano and A. Tassa, 2001: "Cloud-model based Bayesian techniques for precipitation profile retrieval from TRMM microwave sensors". *ECMWF/EuroTRMM* Workshop on Assimilation of Clouds and Precipitation, ECMWF, Reading, U.K., 323-345.

Mugnai A., D. Casella, E. Cattani, S. Dietrich, S. Laviola, V. Levizzani, G. Panegrossi, M. Petracca, P. Sanò, F. Di Paola, D. Biron, L. De Leonibus', D. Melfi, P. Rosci, A. Vocino, F. Zauli, S. Puca, A. Rinollo, L. Milani, F. Porcù, and F. Gattari: Precipitation products from the Hydrology SAF, NHESS, in press, 2013a.

Mugnai A., E. A. Smith, G. J. Tripoli, B. Bizzarri, D. Casella, S. Dietrich, F. Di Paola, G. Panegrossi, P. Sanò, CDRD and PNPR Satellite Passive Microwave Precipitation Retrieval Algorithms: EuroTRMM / EURAINSAT Origins and H-SAF Operations, NHESS, in press, 2013b.

Munchak, S.J., and Kummerow, C.D.: A modular optimal estimation method for combined radar–radiometer precipitation profiling, J. Appl. Meteor. Climat., 50, 433-448, 2011.

Neshyba S.P., T.C. Grenfell and S.G. Warren, 2003: "Representation of a nonspherical ice particle by a collection of independent spheres for scattering and absorption of radiation: 2. Hexagonal columns and plates". *J. Geophys. Res.*, **108**, 4448-4465.

Panegrossi G., S. Dietrich, F.S. Marzano, A. Mugnai, E.A. Smith, X. Xiang, G.J. Tripoli, P.K. Wang and J.P.V. Poiares Baptista, 1998: "Use of cloud model microphysics for passive microwave-based precipitation retrieval: Significance of consistency between model and measurement manifolds". *J. Atmos. Sci*., **55**, 1644-1673.

Panegrossi, G., "Validation of Microphysics Parameterization in Cloud Resolving Models using Passive Microwave Measurements," Ph.D. Dissertation, Univ. of Wisconsin, Madison, WI, UW MET Publication No.04.00.P1, 2004.

Pierdicca N., F.S. Marzano, G. D'Auria, P. Basili, P. Ciotti and A. Mugnai, 1996: "Precipitation retrieval from the spaceborne microwave radiometers based on maximum a posteriori probability estimation". *IEEE Trans. Geosci. Remote Sens*., 34, 831-846.

Prodi F., L. Levi, O. B. Nasello, and L. Lubart, "Morphology and density of ice accreted on cylindrical collectors at low values of impaction parameter. II: Rotating depositsxs," *Q. J. Roy. Meteor. Soc.,* vol. 117, pp. 783-801, 1991.

Roberti L., J. Haferman and C. Kummerow, 1994: "Microwave radiative transfer through horizontally inhomogeneous precipitating clouds". *J. Geophys. Res*., **99**, 16707-16718.

Rosenkranz, P., 2003: Rapid Radiative Transfer Model for AMSU/HSB Channels, IEEE Trans. Geosci. Rem. Sens., 41, 362-368.

Sanò, P., Casella, D., Mugnai, A., Schiavon, A., Smith, E.A., and Tripoli, G.J.: Transitioning from CRD to CDRD in Bayesian retrieval of rainfall from satellite passive microwave measurements, Part 1: Algorithm description and testing, *IEEE Trans. Geosci. Remote Sens*., PP, no.99, pp.1-25, 2013.

Schlűssel P. and H. Luthardt, 1991, "Surface Wind Speeds Over the North Sea From Special Sensor Microwave/Imager Observations". *J. Geophys. Res*., vol. 96, No. C3, 4845-4853.

Skofronick-Jackson G., M.-J. Kim, J.A. Weinman and D.-E. Chang, 2004: "A physical model to determine snowfall over land by microwave radiometry". *IEEE Trans. Geosci Remote Sens.*, in press.

Smith E.A., A. Mugnai, H.J. Cooper, G.J. Tripoli and X. Xiang, 1992: "Foundations for statistical-physical precipitation retrieval from passive microwave satellite measurements. Part I: Brightness-temperature properties of a time-dependent cloud-radiation model". *J. Appl. Meteor.*, **31**, 506-531.

Smith E.A., C. Kummerow and A. Mugnai, 1994a: "The emergence of inversion-type profile algorithms for estimation of precipitation from satellite passive microwave measurements". *Remote Sens. Rev.*, **11**, 211-242.

Smith E.A., X. Xiang, A. Mugnai and G.J. Tripoli, 1994b: "Design of an inversion-based precipitation profile retrieval algorithm using an explicit cloud model for initial guess microphysics". *Meteorol. Atmos. Phys.*, **54**, 53-78.

Smith, E. A., P. Bauer, F. S. Marzano, C. D. Kummerow, D. McKague, A. Mugnai, and G. Panegrossi, "Intercomparison of microwave radiative transfer models for precipitating clouds," *IEEE Trans. Geosci. Remote Sens,* vol. 40, pp. 541-549, 2002.

Smith E.A., Hester W.-Y. Leung, James B. Elsner, Amita V. Mehta, Gregory J. Tripoli,Daniele Casella, Stefano Dietrich, Alberto Mugnai, Giulia Panegrossi, Paolo Sanò: Transitioning from CRD to CDRD in Bayesian Retrieval of Rainfall from Satellite Passive Microwave Measurements: Part 3. Identification of Optimal Meteorological Tags, NHESS, in press, 2013

Surussavadee C., 2006: "Passive Millimeter-Wave Retrieval of Global Precipitation Utilizing Satellites and a Numerical Weather Prediction Model". *Graduation thesis*, MIT Department of Electrical Engineering and Computer Science.

Surussavadee C. and D.H. Staelin, 2006: "Comparison of AMSU millimeterwave satellite observations, MM5/TBSCAT predicted radiances, and electromagnetic models for hydrometeors". *IEEE Trans. Geosci. Remote Sens.*, **44**, 2667-2678.

Surussavadee, C., and Staelin, D.H.: Global millimeter-wave precipitation retrievals trained with a cloud-resolving numerical weather prediction model, Part I: Retrieval design, IEEE Trans. Geosci. Remote Sens., 46, 99-108, 2008a.

Surussavadee, C., and Staelin, D.H.: Global millimeter-wave precipitation retrievals trained with a cloud-resolving numerical weather prediction model, Part II: Performance evaluation, IEEE Trans. Geosci. Remote Sens., 46, 109-118, 2008b.

Surussavadee, C., and Staelin, D.H.: Satellite retrievals of Arctic and Equatorial rain and snowfall rates using millimeters wavelengths, IEEE Trans. Geosci. Remote Sens., 47, 3697-3707, 2009.

Tassa A., S. Di Michele, A. Mugnai, F.S. Marzano, P. Bauer and J.P.V. Poiares Baptista, 2004: "Evaluation of cloud-radiation modeling errors for space-borne passive microwave retrieval of precipitation". *IEEE Trans. Geosci Remote Sens.*, 44,1, 78-89.

Tassa A., S. Di Michele, A. Mugnai, FS. Marzano and J.P.V. Poiares Baptista, 2003: "Cloud-model based Bayesian technique for precipitation profile retrieval from TRMM Microwave Imager". *Radio Sci*., **38**, 8074-8086.

Tripoli G.J. and W.R. Cotton, 1981: "The use of ice-liquid water potential temperature as a thermodynamic variable in deep atmospheric models". *Mon. Wea. Rev.*, **109,** 1094-1102.

Tripoli G.J. and W.R. Cotton, 1982: "The Colorado State University three-dimensional cloud / mesoscale model-1982. Part I: General theoretical framework and sensitivity experiments". *J. Rech. Atmos*. **16:** 185-200.

Tripoli G.J. and W.R. Cotton, 1986: "An intense, quasi-steady thunderstorm over mountainous terrain, part IV: three-dimensional numerical simulation". *J. Atmos. Sci*., **43,** 894-912.

Tripoli G.J., 1992a: "A non-hydrostatic model designed to simulate scale interaction". *Mon. Wea. Rev.*, **120**, 1342-1359.

Tripoli G.J., 1992b: "An explicit three-dimensional non-hydrostatic numerical simulation of a tropical cyclone". *Meteor. Atmos. Phys.*, **49**, 229-254.

Tripoli G. J. and Smith E.A., 2012: "Introducing variable-step topography (VST) coordinates in dynamically constrained, scalable, nonhydrostatic atmospheric models: Review of rationale and solutions on classical obstacle flow calibration problems. ," *Dyn. Atmos. Oceans,* vol. Submitted.

Wiscombe W.J., 1980: "Improved Mie scattering algorithms". *Appl. Opt*., **19**, 1505-1509.

Annex 1: Introduction to H-SAF

The EUMETSAT Satellite Application Facilities

H-SAF is part of the distributed application ground segment of the "*European Organization for the Exploitation of Meteorological Satellites (EUMETSAT)*". The application ground segment consists of a "*Central Application Facilities*" located at EUMETSAT Headquarters, and a network of eight "*Satellite Application Facilities (SAFs)*", located and managed by EUMETSAT Member States and dedicated to development and operational activities to provide satellite-derived data to support specific user communities (see Figure 17):

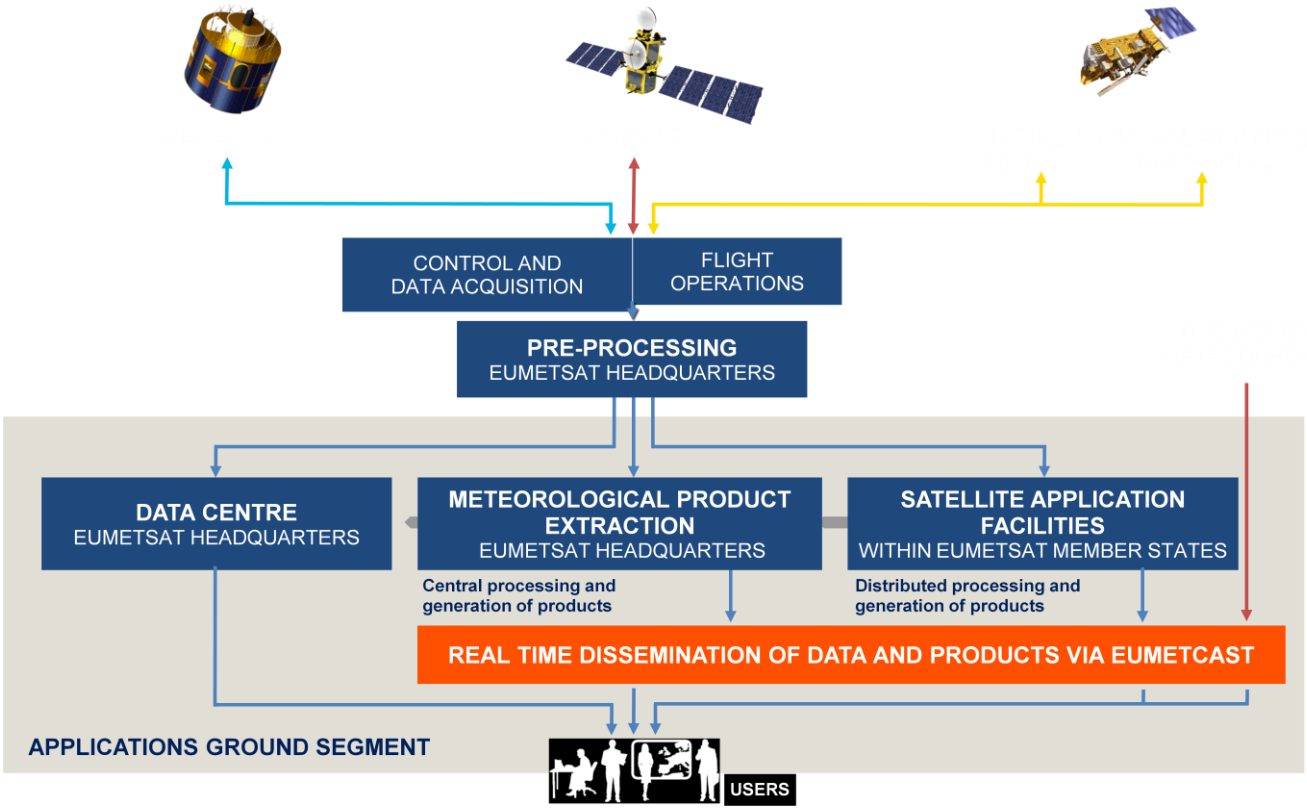

Figure 17: Conceptual scheme of the EUMETSAT Application Ground Segment

Figure here following, depicts the composition of the EUMETSAT SAF network, with the indication of each SAF's specific theme and Leading Entity.

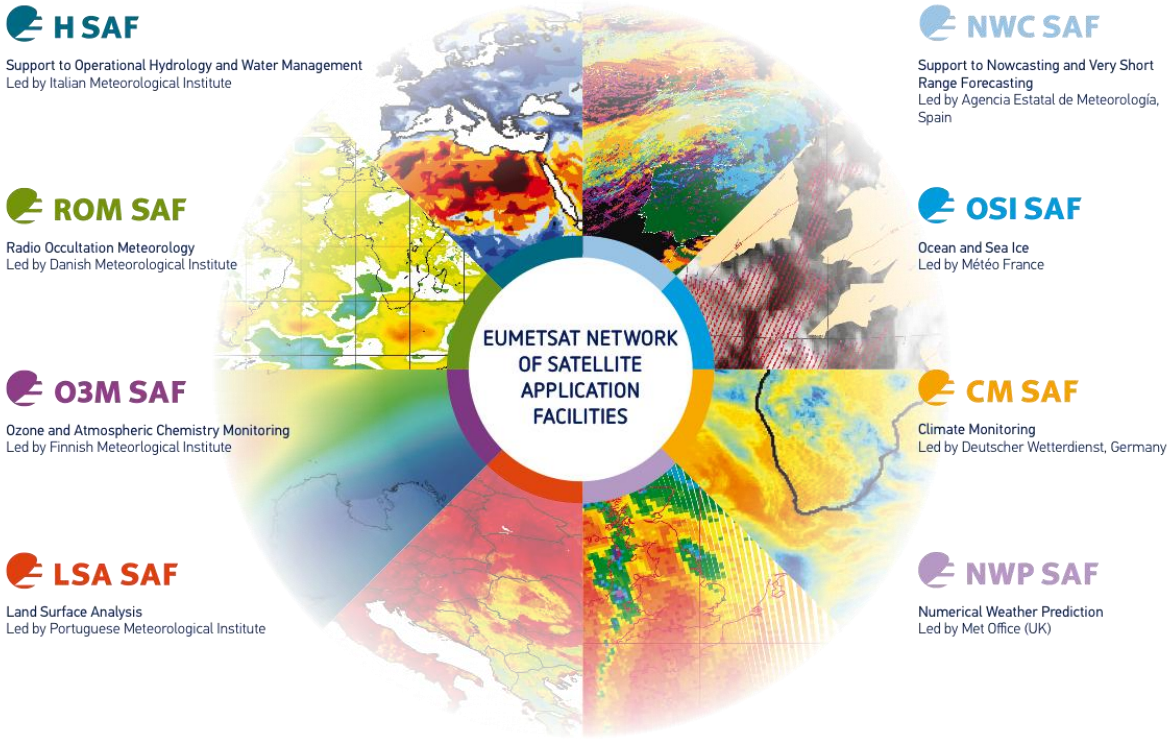

Figure 18: Current composition of the EUMETSAT SAF Network

Purpose of the H-SAF

The main objectives of H-SAF are:

a. ***to provide new satellite-derived products*** from existing and future satellites with sufficient time and space resolution to satisfy the needs of operational hydrology, by generating, centralizing, archiving and disseminating the identified products:

- precipitation (liquid, solid, rate, accumulated);
- soil moisture (at large-scale, at local-scale, at surface, in the roots region);
- snow parameters (detection, cover, melting conditions, water equivalent);

b. ***to perform independent validation of the usefulness of the products*** for fighting against floods, landslides, avalanches, and evaluating water resources; the activity includes:

- downscaling/upscaling modelling from observed/predicted fields to basin level;
- fusion of satellite-derived measurements with data from radar and raingauge networks;
- assimilation of satellite-derived products in hydrological models;
- assessment of the impact of the new satellite-derived products on hydrological applications.

Products / Deliveries of the H-SAF

For the full list of the Operational products delivered by H-SAF, and for details on their characteristics, please see H-SAF website hsaf.meteoam.it.

All products are available via EUMETSAT data delivery service (EUMETCast, http://www.eumetsat.int/website/home/Data/DataDelivery/EUMETCast/index.html), or via ftp download; they are also published in the H-SAF website hsaf.meteoam.it.

All intellectual property rights of the H-SAF products belong to EUMETSAT. The use of these products is granted to every interested user, free of charge. If you wish to use these products, EUMETSAT's copyright credit must be shown by displaying the words "copyright (year) EUMETSAT" on each of the products used.

System Overview

H-SAF is lead by the Italian Air Force Meteorological Service (ITAF USAM) and carried on by a consortium of 21 members from 11 countries (see website: hsaf.meteoam.it for details).

Following major areas can be distinguished within the H-SAF system context:

- Product generation area;
- Central Services area (for data archiving, dissemination, catalogue and any other centralized services);
- Validation services area which includes Quality Monitoring/Assessment and Hydrological Impact Validation.

Products generation area is composed of 5 processing centres physically deployed in 5 different countries; these are:

- for precipitation products: ITAF CNMCA (Italy);
- for soil moisture products: ZAMG (Austria), ECMWF (UK);
- for snow products: TSMS (Turkey), FMI (Finland).

Central area provides systems for archiving and dissemination; located at ITAF CNMCA (Italy), it is interfaced with the production area through a front-end, in charge of product collecting.

A central archive is aimed to the maintenance of the H-SAF products; it is also located at ITAF CNMCA.

Validation services provided by H-SAF consists of:

- Hydrovalidation of the products using models (hydrological impact assessment);
- Product validation (Quality Assessment and Monitoring).

Both services are based on country-specific activities such as impact studies (for hydrological study) or product validation and value assessment.

Hydrovalidation service is coordinated by IMWM (Poland), whilst Quality Assessment and Monitoring service is coordinated by DPC (Italy): The Services' activities are performed by experts from the national meteorological and hydrological Institutes of Austria, Belgium, Bulgaria, Finland, France, Germany, Hungary, Italy, Poland, Slovakia, Turkey, and from ECMWF.